

Climate variability and relationship with ocean fertility during the Aptian Stage

C. Bottini¹, E. Erba¹, D. Tiraboschi¹, H.C. Jenkyns², S. Schouten³, J.S. Sinninghe Damsté³

[1]{Department of Earth Sciences, Università degli Studi di Milano, 20133 Milan, Italy}

[2]{ Department of Earth Sciences, University of Oxford, South Parks Road, Oxford OX1 3AN, UK}

[3]{NIOZ Royal Netherlands Institute for Sea Research, Department of Marine Organic Biogeochemistry, P.O. Box 59, 1790 AB Den Burg Texel, The Netherlands}

Correspondence to: C. Bottini (cinzia.bottini@unimi.it)

Abstract

Several studies have been conducted to reconstruct temperature variations across the Aptian Stage, particularly during the Early Aptian Oceanic Anoxic Event (OAE)1a. There is a general consensus that a major warming characterized the OAE 1a, although some studies have provided evidence for transient ‘cold snaps’ or cooler intervals during the event. The climatic conditions for the middle–late Aptian are less constrained, and a complete record through the Aptian is not available. Here we present a reconstruction of surface-water palaeotemperature and fertility based on calcareous nannofossil records from the Cismon and Piobbico cores (Tethys) and DSDP Site 463 (Pacific Ocean). The data, integrated with oxygen-isotope and TEX₈₆ records, provide a detailed picture of climatic and ocean fertility changes during the Aptian Stage, which are discussed in relation to the direct/indirect role of volcanism. Warm temperatures characterized the pre-OAE 1a interval followed by a

maximum warming (of ~2–3 °C) during the early phase of anoxia under intense volcanic activity of the Ontong Java Plateau (OJP). A short-lived (~35ky) cooling episode interrupted the major warming, following a rapid increase of weathering rates. Nannofossils indicate that eutrophic conditions were reached when temperatures were at their highest and OJP volcanism most intense, thus suggesting that continental runoff, together with increased input of hydrothermal metals, increased nutrient supply to the oceans. The latter part of OAE 1a was characterized by cooling events, probably promoted by CO₂ sequestration during burial of organic matter. In this phase, high productivity was probably maintained by N₂-fixing cyanobacteria while nannofossil taxa indicating high fertility were rare. The end of anoxia coincided with the cessation of volcanism and a pronounced cooling. The mid-Aptian was characterized by high surface-water fertility and progressively decreasing temperatures, probably resulting from intense continental weathering drawing down *p*CO₂. The lowest temperatures, combined with low fertility, were reached in the middle–late Aptian across the interval characterized by blooming of *Nannoconus truittii*. The data presented suggest that OJP activity played a direct role in inducing global warming during the early Aptian, whereas other mechanisms (weathering, deposition of organic matter) acted as feedback processes, favouring temporary cooler interludes.

1 Introduction

The Aptian (~121 to ~113 Ma, Malinverno et al., 2012) has been characterized by climatic changes and profound environmental perturbations including the Oceanic Anoxic Event 1a (OAE 1a: ~120 Ma), representing a global phenomenon of organic-matter burial in oxygen-depleted oceans. The disturbance in the carbon cycle related to OAE 1a is recorded in sedimentary successions worldwide, presenting a negative carbon-isotope anomaly at the onset of OAE 1a, followed by a positive excursion that extends into the late Aptian (e.g. Weissert, 1989; Weissert and Lini, 1991; Jenkyns, 1995; Menegatti et al., 1998; Bralower et al., 1999; Erba et al., 1999; Luciani et al., 2001; Bellanca et al., 2002; Price, 2003; van Breugel et al., 2007; Ando et al., 2008; Méhay et al., 2009; Malkoč et al., 2010; Mahanipour et al., 2011; Millán et al., 2011; Stein et al., 2011; Bottini et al., 2012; Hu et al., 2012). Volcanism, associated with the emplacement of the Ontong Java Plateau (OJP), is thought to be the main triggering mechanism for global anoxia as well as for imposed greenhouse conditions and ocean acidification during OAE 1a (e.g. Larson, 1991; Erba, 1994; Bralower et


al., 1994; Larson and Erba, 1999; Jones and Jenkyns, 2001; Leckie et al., 2002; Jenkyns, 2003; Méhay et al., 2009; Tejada et al., 2009; Erba et al., 2010; Bottini et al., 2012)

Several studies are suggestive of significant temperature increase during OAE 1a, as recorded by different temperature proxies (i.e. oxygen isotopes, TEX₈₆, calcareous nannofossils, palynomorphs) in the Tethys (e.g. Menegatti et al., 1998; Hochuli et al., 1999; Luciani et al., 2001; Bellanca et al., 2002; Jenkyns, 2003; Millán et al., 2009; Erba et al., 2010; Jenkyns, 2010; Keller et al., 2011; Stein et al., 2011; Bottini et al., 2012; Hu et al., 2012; Husinec et al., 2012), Vocontian Basin (e.g. Moullade et al., 1998; Kuhnt et al., 2011), Lower Saxony Basin (Mutterlose et al., 2010; Bottini and Mutterlose, 2012; Pauly et al., 2013), North Sea (Mutterlose and Bottini, 2013), eastern European Russian Platform (Zakharov et al., 2013), Pacific (e.g. Jenkyns, 1995; Price, 2003; Schouten et al., 2003; Ando et al., 2008; Bottini et al., 2012), and Atlantic Oceans (e.g. Tremolada et al., 2006). Some works have provided evidence for a climatic variability during OAE 1a, identifying short-lived cooling events (e.g. Dumitrescu et al., 2006; Keller et al. 2011; Kuhnt et al., 2011; Jenkyns et al., 2012; Lorenzen et al., 2013). At the end of OAE 1a, a temperature decline is registered in the Tethys (e.g. Weissert and Lini, 1991; Menegatti et al., 1998; Hochuli et al., 1999; Luciani et al., 2001; Bellanca et al., 2002; Millán et al., 2009), Vocontian Basin (e.g. Herrle et al., 2010; Kuhnt et al., 2011), Boreal Realm (e.g. Rückheim et al., 2006; Malkoč et al., 2010; Bottini and Mutterlose, 2012; Pauly et al., 2013; Mutterlose and Bottini, 2013), and Pacific Oceans (e.g. Jenkyns, 1995; Jenkyns and Wilson, 1999; Price, 2003; Dumitrescu et al., 2006; Ando et al., 2008).

For the late Aptian, cooler conditions have been reconstructed based on migration of boreal species southwards (e.g. Herrle and Mutterlose, 2003; Mutterlose et al., 2008), oxygen-isotope records (e.g. Weissert and Lini, 1991; Jenkyns, 1995; Hu et al., 2012; Price, 2012; Maurer et al., 2012), putative ice-rafted debris in high latitudes (Kemper 1987; Frakes and Francis 1988; De Lurio and Frakes 1999; Price, 1999) and, for sea-bottom temperatures, the presence of glendonites (marine low-temperature hydrated polymorphs of calcium carbonate), (Kemper 1987). Recently McAnena et al. (2013) have documented, on the basis of TEX₈₆ data, a ~2 Myr long interval of relatively cool conditions (~ 28-29 °C) in the late Aptian in the Proto-North Atlantic followed by a warming (up to ~31 °C), linked to OAE 1b.

Although the amount of information about temperature variations across the Aptian is considerable, a complete picture of climatic changes is not available. In most cases, the

records are poorly correlated between the different basins and/or cover limited time intervals within the ~12 My-long Aptian Stage (Malinverno et al., 2012). In this work, we focus primarily on surface-water temperatures through the Aptian reconstructed on the basis of calcareous nannofossils from three well sites: Cismon (Italian Southern Alps), Piobbico (Umbria–Marche Basin, central Italy) and DSDP Site 463 (Mid-Pacific Mountains). The existing stratigraphic framework for the three sites and available cyclochronology for the Cismon core (Malinverno et al., 2010), allow high-resolution dating of climatic fluctuations. Calcareous nannoplankton live in the (upper) photic zone and are a good proxy of present and past surface-water conditions, being sensitive to temperature, fertility, salinity and $p\text{CO}_2$ (Mutterlose et al., 2005). Extant calcareous nannoplankton occur from coastal areas to the open ocean, although with different abundance and diversity and, together with diatoms, dinoflagellates and bacteria constitute marine phytoplanktonic communities. The Mesozoic geological record confirms the wide geographical/latitudinal distribution of calcareous nannofossils (coccoliths and nannoliths) that are commonly used to trace palaeoecological conditions. Within nannofossil assemblages, nannoconids are inferred to have been restricted to the deep photic zone at the base of the mixed layer on top of the thermocline coinciding with a deep nutricline (Erba, 1994). In the studied intervals, nannoconids are relatively scarce, and micrite mostly consists of coccoliths, thus essentially recording the uppermost water masses.

 In this work, stable carbon and oxygen isotopes on bulk rock have been measured to reconstruct changes in surface-water temperature, taking into account potential diagenetic modification. The preservation of nannofossils provides information on the early diagenetic history of pelagic carbonates, (Erba, 1992b; Herrle et al., 2003; Tiraboschi et al., 2009). Although oxygen-isotope ratios contain a mixing of a primary signal and later diagenetic phases (Marshall, 1992), hampering the use of palaeotemperature values, the $\delta^{18}\text{O}$ bulk data can be used to derive trends toward warmer/cooler conditions. New oxygen-isotope data for DSDP Site 463 and Piobbico have been generated, and are directly correlated with calcareous nannofossil variations as well as with new TEX_{86} data from the Cismon core.

The aims of our work are to: a) trace climatic variations during the Aptian Stage; b) reconstruct, in high resolution, the climate variability through OAE 1a; c) identify synchronicity and diachronicity of temperature variations in different oceanic basins; c) trace

the direct/indirect role of volcanism, weathering rates and $p\text{CO}_2$ on climate changes connected with OAE 1a and its aftermath.

We also characterize the evolution of surface-water fertility during the Aptian Stage. Previous studies (e.g. Coccioni et al., 1992; Bralower et al. 1993; Erba, 1994, 2004; Premoli Silva et al., 1999; Leckie et al., 2002; Mutterlose et al., 2005; Tremolada et al., 2006; Bottini and Mutterlose, 2012) mainly focused on the OAE 1a interval, documenting an increase in surface-water fertility accompanied by high primary productivity, but a record throughout the entire Aptian is missing. We therefore highlight fluctuations in fertility during and after OAE 1a, identifying potential relationships with climatic changes on both the short- and the long-term as well as oceanic nutrification.

2 Material and methods

2.1 Studied sites

We have investigated the Upper Barremian–Aptian interval at three sites in the Tethys and Pacific Oceans (Figure 1):

The **Cismon core**, drilled in the Southern Alps, north-eastern Italy ($46^{\circ}02'N$; $11^{\circ}45'E$; 398 m altitude) is represented by a total stratigraphic thickness of 131.8 m with 100% recovery. The site was located on the southern margin of the Mesozoic Tethys, on the eastward deepening slope between the Trento Plateau (a pelagic submarine high) and the Belluno Basin (Erba and Tremolada, 2004). The Cismon sequence was deposited at an estimated palaeo-depth of 1000–1500 m during the Early Cretaceous (Weissert and Lini, 1991; Erba and Larson 1998; Bernoulli and Jenkyns, 2009). In the uppermost part of the cored section (at 7.80 m) there is a major hiatus corresponding to the late Aptian and the early–middle Albian. The Selli Level (sedimentary expression of OAE 1a) is represented by a ~5 m-thick interval, between 23.67 and 18.64 stratigraphic metre depths (Erba and Larson, 1998; Erba et al., 1999). Lithologically, the Selli Level is characterized by marlstones alternating with black shales and discrete radiolarian-rich beds (Coccioni et al., 1987; Erba et al., 1999). The interval studied extends from 35 m to 10 m.

The **Piobbico core** was drilled at “Le Breccie” ($43^{\circ}35'3.78''N$; $12^{\circ}29'10.09''E$), located 3 km west of the town of Piobbico (Marche, Italy), at Km 33 of the Apecchiese State Road No.

257, on the left hydrographic side of the Biscubio stream. Coring penetrated the entire Marne a Fucoidi Formation, including the upper transition to the Scaglia Bianca and the lower transition to the Maiolica. The total length of the core is 84 m with 98.8% recovery; after adjusting for dip direction, the stratigraphic thickness equals 77 m. The lithostratigraphy and calcareous plankton biostratigraphy of the core were described by Erba (1988, 1992a) and Tornaghi et al. (1989). The Selli Level, consisting of black shales and radiolarian-rich beds, extends from 75.94 to 73.47 m. The interval studied covers the interval from 77 m to 40 m.


DSDP Site 463 was drilled at a water depth of 2525 m on the ancient structural high of the western Mid-Pacific Mountains (21°21.01'N, 174°40.07'E) during DSDP Leg 62. During the Early Cretaceous, Site 463 was located at a palaeo-latitude of ~20°S, with a palaeo-depth between a few hundred metres (Mélières et al., 1978) and ~1 km (Roth, 1981). The Selli Level equivalent is located between ~626 and 615 mbsf, corresponding to ~12 m of tuffaceous limestones containing a number of discrete organic-rich horizons (Thiede et al., 1981; Erba, 1994). The interval studied covers from 650 to 515 mbsf.

2.2 Calcareous nannofossils

Calcareous nannofossils were investigated under polarizing light microscope at 1250X magnification in smear slides and thin-sections. Smear slides were prepared using standard techniques, without centrifuging or cleaning in order to retain the original sedimentary composition. A small quantity of rock was powdered in a mortar with bi-distillate water and mounted on a glass slide with Norland Optical Adhesive. A total of 285 smear slides for the Cismon core, 179 smear slides for the Piobbico core and 281 smear slides for DSDP Site 463 were investigated. At least 300 nannofossil specimens were counted in each sample and percentages of single taxa were calculated relative to the total nannoflora.

Thin-sections were polished to an average thickness of 7µm for optimal view of nannofossils; a total of 85 thin-sections for the Cismon Core (which integrates the data from Erba and Tremolada, 2004), 242 for DSDP Site 463, and 179 for Piobbico core were investigated. Absolute abundances were obtained by counting all nannofossil specimens in 1 mm² of the thin-section.

2.3 Statistical analysis

The software “Statsoft Statistica 6” was used for multivariate “factor analysis” (FA) (R-mode) varimax rotation with principal component extraction to determine the relationships between samples and variables, and to identify palaeoceanographic and palaeoecological affinities among selected nannofossil taxa. Factor loadings represent relationships among individual taxa within the main factors, whereas factor scores denote the relationships within the sampled cases (lithological samples). The same software was used for the “principal components and classification analysis” (PCCA) and $\delta^{18}\text{O}$ values. The species used in FA and PCCA statistical analyses (*Watznaueria barnesiae*, *Biscutum constans*, *Discorhabdus rotatorius*, *Zeugrhabdotus erectus* , *Rhagodiscus asper*, *Zeugrhabdotus diplogrammus*, *Stauroolithites stradneri*, *Repagulum parvidentatum*, *Eprolithus floralis*, *Nannoconus* sp. and *Cretarhabdus surirellus*) have been selected on the basis of their palaeoecological significance (e.g. Roth and Krumbach, 1986; Erba, 1992b; Herrle et al., 2003; Mutterlose et al., 2005; Tiraboschi et al., 2009).

2.4 Oxygen-isotope analysis

New oxygen stable-isotope analyses were performed at Oxford University on bulk carbonate fraction of 57 samples from DSDP Site 463 and of 373 samples from Piobbico. Bulk-rock samples for isotopic analysis were first powdered, cleaned with 10% H_2O_2 followed by acetone, and then dried at 60°C. Powders were then reacted with purified orthophosphoric acid at 90°C and analyzed online using a VG Isocarb device and Prism Mass Spectrometer. Long-term reproducibility, as determined from repeat measurements of the in-house standard (Carrara marble), resulted in analytical uncertainties of $\delta^{18}\text{O} = -1.86 \pm 0.1$. The values are reported in the conventional delta notation with respect to the Vienna Pee Dee Belemnite (V-PDB) standard. For DSDP Site 463 data are drawn from Price (2003), Ando et al. (2008) and this work, and for the Cismon core $\delta^{18}\text{O}$ come from Méhay et al. (2009) and Erba et al. (2010).

2.5 TEX_{86}

Sediments from the Cismon core were extracted as described by van Breugel et al. (2007). The polar fractions of the extracts, containing the GDGTs, were dried under a stream of nitrogen (N_2) redissolved by sonication (5 min) in 200 μl hexane/propanol (99:1; vol:vol),

and filtered through 0.45 μm polytetrafluoroethylene (PTFE) filters. GDGTs were analyzed by high-pressure liquid chromatography–mass spectrometry (HPLC/MS) following the method described by Schouten et al. (2007). Samples were analyzed on an Agilent 1100 series LC/MSD SL. A Prevail Cyano column (150 mm \times 2.1 mm, 3 mm) was used with hexane:propanol (99:1; vol:vol) as an eluent. After the first 5 min, the eluent increased by a linear gradient up to 1.8% isopropanol (vol) over the next 45 min at a flow rate of 0.2 mL min⁻¹. Identification and quantification of the GDGTs isomers was achieved by integrating the peak areas of relevant peaks in m/z 1300, 1298, 1296, 1292, 1050, 1036 and 1022 selected ion monitoring scans. The TEX₈₆ ratio was calculated following Schouten et al. (2002):

$$\text{TEX}_{86} = ([\text{GDGT 2}] + [\text{GDGT 3}] + [\text{crenarchaeol regioisomer}]) / ([\text{GDGT 1}] + [\text{GDGT 2}] + [\text{GDGT 3}] + [\text{crenarchaeol regioisomer}]) \quad (1)$$

where numbers correspond to isoprenoid GDGTs from marine Thaumarchaeota with 1, 2 or 3 cyclopentane moieties, and the crenarchaeol regioisomer has the antiparallel configuration of crenarchaeol (Sinninghe Damsté et al., 2002).

The TEX₈₆ values were converted to SST using the most recent core-top calibration as proposed by Kim et al. (2010) for oceans with SST > 15°C:

$$\text{SST} = 38.6 + 68.4 \times \log (\text{TEX}_{86}) \quad (2)$$

The Branched and Isoprenoid Tetraether (BIT) index is based on the relative abundance of non-isoprenoidal GDGTs derived from soil bacteria versus a structurally related isoprenoid GDGT, ‘crenarchaeol’ with four cyclopentane moieties and one cyclohexane moiety, produced by marine Thaumarchaeota. The BIT index, which thus represents a measure for soil versus marine organic matter input in marine sediments, was calculated according to Hopmans et al. (2004):

$$\text{BIT} = ([\text{GDGT-I}] + [\text{GDGT-II}] + [\text{GDGT-III}]) / ([\text{Crenarchaeol}] + [\text{GDGT-I}] + [\text{GDGT-II}] + [\text{GDGT-III}])$$

3 Stratigraphic framework

In this work, the stratigraphic framework for the three cores investigated is based on carbon-isotope stratigraphy calibrated with calcareous nannofossil and foraminiferal biostratigraphy. For the Cismon core and DSDP Site 463, magnetic chron CM0 has been used to define the base of the Aptian; this level was not reached with the Piobbico core.

In addition to the two well-known, high-amplitude $\delta^{13}\text{C}$ Aptian excursions, several minor fluctuations are identified in the carbon-isotope record from the Tethys, Pacific and Atlantic Oceans, which allow codification of major and minor perturbations. Menegatti et al. (1998) focused on the late Barremian–early Aptian interval and identified segments C1–C8. Subsequently, Bralower et al. (1999) extended the codification of Menegatti et al. (1998) through the rest of the Aptian Stage (C1–C11). Herrle et al. (2004) introduced new codes for the Aptian starting from Ap6, coinciding with C5 and C6 of Menegatti et al. (1998), to Al2. McAnena et al. (2013) used the Ap9–Al3 segments previously identified by Herrle et al. (2004).

The studied sections cover the latest Barremian to earliest Albian time interval. We revised the Herrle et al. (2004) carbon-isotope segments by extending their codes down to Ap1 and renaming the earliest Albian fluctuations Al1 to Al3. Segments Ap1–Ap7 coincide with previously identified segments C1–C7 (Menegatti et al., 1998). The $\delta^{13}\text{C}$ curve for the rest of the Aptian shows several fluctuations, allowing a higher resolution subdivision into segments Ap8–Ap18. In this paper, we applied a double coding for Ap1/C1 through Ap7/C7 segments and used the new Ap8–Ap18 and Al1–Al3 codes for the late Aptian–earliest Albian time interval. At Cismon, we identify segments Ap1–Ap8, at Piobbico Ap2–Al3, and at DSDP Site 463 Ap1–Ap15. Segments Ap8–Ap15 are less well defined at DSDP Site 463 due to incomplete core recovery.


In addition to nannofossil zones NC6–NC8 (Bralower et al., 1995), we used the “nannoconid decline” and the “nannoconid crisis” (e.g. Erba et al., 2010) as further bio-horizons. Moreover, in the late Aptian the “*Nannoconus truittii* acme” (Mutterlose, 1989; Erba, 1994; Herrle and Mutterlose, 2003), defines a globally recognized interval where *N. truittii* dominates the assemblages with abundances from 5 up to 40 % of the total nannofloras.

As far as lithostratigraphy is concerned, the Selli Level or its equivalents are identified at all three sites. A lithological revision of the Piobbico core also allowed the identification of the Kilian Level Equivalent, corresponding to the prominent black shale at the bottom of lithological Unit 12 within core 44 (Erba, 1988). The Kilian level Equivalent in the Piobbico core is characterized by very fine laminations, without bioturbation, and has a thickness of 33 cm (from 45.13 to 44.80 m). Following Petrizzo et al. (2012), the Kilian Level marks the Aptian/Albian boundary.

Regarding the Piobbico core, we identify the presence of a hiatus that eliminates part of the basal Selli Level. In particular, on the basis of the correlation between the lithology and carbon-isotope record from the Piobbico core with the equivalent records from the Cismon core and DSDP Site 463 (Figure 2), as well as from other sedimentary basins, we note that: 1) the $\delta^{13}\text{C}$ values from 75.94 to 74.80 m, ranging between 2 and 3 ‰, probably correspond to segments Ap4/C4 and Ap5/C5 rather than to the negative excursion Ap3/C3 where values of Cismon and DSDP Site 463 sediments are below 1‰; 2) $\delta^{18}\text{O}$ values from 75.94 to 74.80 m fall between -3 and -1‰ and never reach the highly negative values (-4‰) characteristic of those in the Ap3/C3 segment of the other two sites, but rather conform to the range of values detected in segments Ap4/C4 and Ap5/C5; 3) the Selli Level in the Cismon core is characterized by three lithological sub-units (Erba et al., 1999), the lowermost being represented by laminated black shales corresponding to segment Ap3/C3, the second characterized by prevailing light grey marlstones corresponding to segments Ap4/C4 and Ap5/C5, and the uppermost one characterized by laminated black shales corresponding to segment Ap6/C6. The total organic carbon content (TOC) in the Cismon core shows highest values corresponding to segments Ap4/C, the base of segment Ap5/C5, as well as segment Ap6/C6. Similar high values are detected at DSDP Site 463 in coeval stratigraphic positions. At Piobbico, only two lithological sub-units are recognized (Erba, 1988) following the definition of Coccioni et al. (1987, 1989). The lower part, namely the “green interval”, is dominated by light green claystones, while the upper “black interval” is characterized by laminated black shales. It is therefore possible that the lowermost black shale interval normally found in the Selli Level equivalents is missing at Piobbico and only the other two lithostratigraphic intervals, corresponding to Ap4/C4-Ap5/C5 and Ap6/C6, respectively, are represented.

4 Results

4.1 Calcareous nannofossil abundances

Figures 3–5 illustrate the distribution of the high-fertility (*D. rotatorius*, *B. constans*, *Z. erectus*) and low-fertility (*W. barnesiae*) nannofossil taxa (following Roth and Krumbach, 1986; Premoli Silva et al., 1989a, 1989b; Watkins, 1989; Coccioni et al., 1992; Erba et al., 1992b; Williams and Bralower, 1995; Bellanca et al., 1996; Herrle, 2002, 2003; Herrle et al., 2003; Bornemann et al., 2005; Mutterlose et al., 2005; Tremolada et al., 2006; Tiraboschi et al., 2009), as well as of the warm-temperature (*R. asper*, *Z. diplogrammus*) and cool-temperature (*S. stradneri*, *E. floralis*, *R. parvidentatum*) taxa (following Roth and Krumbach, 1986; Wise, 1988; Erba, 1992b; Erba et al., 1992; Mutterlose, 1992; Herrle and Mutterlose, 2003; Herrle et al., 2003; Tiraboschi et al., 2003 

A description of the major trends of these taxa is given for the three sections investigated:

In the **Cismon core** (Fig. 3), *W. barnesiae* is the dominant species with mean abundance of 66.8%. *Rhagodiscus asper* ranges from 0 to 20% of the total assemblage (mean: 3%) showing the highest peaks in the lowermost part of the Selli Level (segments Ap3/C3 and Ap4/C4 of the carbon-isotope curve). *Zeugrhabdotus diplogrammus* ranges from 0 to 2% (mean: 0.1%). *Staurolithites stradneri* ranges from 0 to 4% (mean: 0.2%), and shows peaks in the uppermost part of the Selli Level (segment Ap6/C6). *Eprolithus floralis* ranges from 0 to 6% (mean: 0.2%) and shows peaks just above the top of the Selli Level (Ap7/C7). *Biscutum constans* ranges from 0 to 2% (mean: 0.2%), *D. rotatorius* from 0 to 3.5% (mean: 0.4%), and *Z. erectus* from 0 to 4.1% (mean: 0.15%). These three species are more abundant in the lower part of the Selli Level (segments Ap3/C3, Ap4/C4 and part of Ap5/C5). Nannoconids show a decline in abundance starting prior to magnetic chron CM0 (where they show high abundances up to 40% in smear slides; $1 \cdot 10^4$ specimens/mm² in thin-section) and reaching a minimum corresponding with segment Ap3/C3 of the carbon-isotope curve where they are virtually absent.

In the **Piobbico core** (Fig. 4), the interval from 75.29 to 73.92 m, within the Selli Level, is barren of calcareous nannofossils. In the rest of studied interval, *Watznaueria barnesiae* is the dominant species with a mean abundance of 62%. *Rhagodiscus asper* ranges from 0 to 7.7% (mean: 2.4%). *Zeugrhabdotus diplogrammus* fluctuates between 0 and 1.2% (mean: 1%). *Eprolithus floralis* ranges from 0 to 3.5% (mean: 0.5%), *R. parvidentatum* from 0 to 0.3%

(mean: 0.04%), and *S. stradneri* from 0 to 3% (mean: 0.6%); these taxa are more abundant above the Selli Level, showing the highest values in corresponding with segments Ap11, Ap13–Ap15 of the carbon-isotope curve. *Biscutum constans* ranges from 0 to 4.1% (mean: 0.1%), *D. rotatorius* from 0 to 20% (mean: 2.7%), and *Z. erectus* from 0 to 6.5% (mean: 0.9%). The latter three species are more abundant corresponding with segments Ap9–Ap11 of the carbon-isotope curve. Nannoconids are absent to rare throughout most of the studied interval except for an interval between 60.37 and 55.61 m, where they show rather high abundances (up to 40 % relative abundance in smear slides; 4×10^3 specimens/mm² absolute abundance in thin-section). This particular interval is dominated by *N. truittii* and coincides with the “*N. truittii* acme”.

At **DSDP Site 463** (Fig. 5), the intervals from 624.24 to 623.96 mbsf and from 623.16 to 622.57 mbsf, within the Selli Level, are barren of calcareous nannofossils. *Watznaueria barnesiae* is the dominant species with a mean abundance of 58%. *Rhagodiscus asper* ranges from 0 to 32% (mean: 6.5%), having the highest values in the lower part of the section below the Selli Level Equivalent. *Zeugrhabdotus diplogrammus* ranges from 0 to 2.7% (mean: 1%). *Eprolithus floralis* ranges from 0 to 8.4% (mean: 0.9%) and *S. stradneri* from 0 to 11.15% (mean: 2.0%); both taxa are particularly abundant in levels corresponding to segments Ap12 and part of Ap13. *Biscutum constans* ranges from 0 to 6.7% (mean: 0.6%), *D. rotatorius* from 0 to 30% (mean: 2.4%), and *Z. erectus* from 0 to 16% (mean: 1.2%). These three species are more abundant within the lower part of the Selli Level Equivalent (segments Ap3–Ap4 of the carbon-isotope curve). A peak is also detected around segment Ap8. Nannoconids are abundant below the Selli Level Equivalent and between 568.27 and 540.73 mbsf (segments Ap12 and part of Ap13) showing abundances up to 40 % (relative abundance in smear slides) and 4×10^3 specimens/mm² (absolute abundance in thin-section), dominated by *Nannoconus truittii*, which marks the *Nannoconus truittii* acme interval.

For each studied site, two significant factors were extracted from the FA (R-mode) varimax rotation analysis:

In the **Cismon core** (Fig. 6A, Tab. 1 of Supplementary material), Factor 1 (F1) and Factor 2 (F2) represent 32% of the total variance. F1 (19% of the total variance) shows the highest positive loadings for *W. barnesiae* and the highest negative loadings for *D. rotatorius*, *B. constans*, *Z. erectus*. F2 (13% of the total variance) shows positive loadings for *W. barnesiae*,

S. stradneri, *E. floralis*, and negative loadings for *R. asper*, *C. surirellus* and *Z. diplogrammus*. F1 is interpreted to correspond with surface-water fertility and F2 to surface-water temperature, respectively.

In the **Piobbico core** (Fig. 6B, Tab. 2 of Supplementary material). F1 and F2 represent 36% of the total variance. F1 (25% of the total variance) shows high positive loadings for *Z. erectus*, *D. rotatorius*, *B. constans*, *R. irregularis*, *C. surirellus*, *R. asper* and high negative loadings for *Nannoconus* sp. and *W. barnesiae*. F2 (11% of the total variance) shows the highest positive loadings for *W. barnesiae*, *S. stradneri*, *E. floralis* and the highest negative loadings for *Nannoconus* sp. F1 is interpreted to correspond with surface-water fertility and F2 with surface-water temperature, respectively.

At **DSDP Site 463** (Fig. 6C, Tab. 3 of Supplementary material), F1 and F2 represent 36% of the total variance. F1 (17% of the total variance) shows the highest positive loadings for *D. rotatorius*, *Z. diplogrammus*, *B. constans*, *R. irregularis* and the highest negative loadings for *Nannoconus* sp. F2 (19% of the total variance) shows the highest positive loadings for *Nannoconus* sp., *E. floralis*, *S. stradneri* and the highest negative loadings for *W. barnesiae*, *R. asper*, *B. constans*. F1 is interpreted to correspond with surface-water fertility and F2 with surface-water temperature, respectively.

Nannoconids show apparently a different affinity at Piobbico compared to the Cismon and DSDP Site 463 records, being associated with taxa indicator of warm waters and high nutrients, instead of the cold-water species *S. stradneri* and *E. floralis*. However, this discrepancy can be explained with the record of Piobbico starting around the “nannoconid crisis”, thus excluding the latest Barremian–earliest Aptian interval dominated by nannoconids. It is well possible that the results of the FA are in this case not reliable or should be considered with caution.



The results of the PCCA analysis are summarized as follow:

In the **Cismon core** (Fig. 6D, Tab. 4 of Supplementary material), the first component (22% of the total variance) shows the highest positive loadings for *D. rotatorius*, *B. constans*, *Z. erectus* and the highest negative loadings for *W. barnesiae* and *Nannoconus* sp. The second component (15% of the total variance) shows the highest positive loadings for *S. stradneri*, *W. barnesiae* and the $\delta^{18}\text{O}$ (associated variable), and the highest negative loadings for *R. asper*

and *C. surirellus*. The 1 axis is interpreted to correspond with surface-water fertility, the 2 axis to surface-water temperature.

In the **Piobbico core** (Fig. 6E, Tab. 5 of Supplementary material), the first component (28% of the total variance) shows the highest positive loadings for *D. rotatorius*, *B. constans*, *Z. erectus* and the highest negative loadings for *Nannoconus* sp. The second component (11% of the total variance) shows the highest positive loadings for *E. floralis*, *S. stradneri*, *W. barnesiae* and the highest negative loadings for *D. rotatorius*. The associated variable $\delta^{18}\text{O}$ has loadings close to zero. The 1 axis is interpreted to correspond with surface-water fertility, while the interpretation for the 2 axis is not straightforward, but might correspond with surface-water temperature.

The dataset collected in this work for Piobbico core has been integrated with the dataset from Tiraboschi et al. (2009) covering the Albian. The results of the PCCA analysis performed on the integrated dataset are presented in Figure 6F. The first component (32% of the total variance) shows the highest positive loadings for *D. rotatorius*, *B. constans*, *Z. diplogrammus*, *R. asper*, *C. surirellus*, *R. irregularis*, *Z. erectus* and the highest negative loadings for *W. barnesiae* and *Nannoconus* sp.. The second component (13% of the total variance) shows the highest positive loadings for *E. floralis*, *S. stradneri* and *R. parvidentatum* and the highest negative loadings for *R. asper*, *Z. diplogrammus* and *B. constans*. Also the associated variable $\delta^{18}\text{O}$ exhibits positive loadings. The 1 axis is interpreted to correspond with surface-water fertility, while the 2 axis corresponds with surface-water temperature.

At **DSDP Site 463** (Fig. 6G, Tab. 6 of Supplementary material), the first component (24% of the total variance) shows the highest negative loadings for *R. asper*, *Z. erectus*, and lower negative loadings for *S. stradneri*, *E. floralis*. The second component (16% of the total variance) shows the highest positive loadings for *D. rotatorius*, *R. irregularis*, *B. constans*, *Z. erectus*, and negative loadings for *W. barnesiae*, and *Nannoconus* sp., $\delta^{18}\text{O}$ (associated variable) has loadings close to zero. The 1 axis is interpreted to correspond with surface-water temperature, the 2 axis with surface-water fertility.

4.2 Nannofossil Temperature and Nutrient Indices

On the basis of reconstructed nannofossil affinities to temperature and nutrient content of surface waters, some authors (e.g. Herrle et al., 2003; Tiraboschi et al., 2009) have proposed

two indices: the Temperature Index (TI) and the Nutrient Index (NI). According to these palaeoecological reconstructions, and the results of our FA and PCCA analysis, we modified the formulae of Herrle et al. (2003) by excluding taxa that are sparse and rare in the studied sections. The formulae of the indices used here are (4) and (5):

$$TI = (Ss + Ef + Rp) / (Ss + Ef + Rp + Ra + Zd) \times 100 \quad (4)$$

$$NI = (Bc + Dr + Ze) / (Bc + Dr + Ze + Wb) \times 100 \quad (5)$$

Where: *Ss* = *S.stradneri*; *Ef* = *E.floralis*; *Rp* = *R.parvidentatum*; *Ra* = *R.asper*; *Zd* = *Z.diplogrammus*; *Bc* = *B.constans*; *Dr* = *D.rotatorius*; *Ze* = *Z.erectus*; *Wb* = *W.barnesiae*.

The nannofossil TI, calibrated against carbon-isotope stratigraphy, has revealed systematic and synchronous changes in the Cismon core, Piobbico core and at DSDP Site 463. A complete nannofossil record through OAE 1a is available only for the Cismon core, because the Selli Level of the Piobbico core is incomplete and many samples are barren of nannofossils, while at DSDP Site 463 the top of the Selli Level Equivalent is probably not recovered and some samples are barren. In the three investigated sites, the TI and NI show the following fluctuations:

At **Cismon** (Fig. 3) the TI shows high-frequency fluctuations superimposed on a longer term trend. The warmest temperatures were reached in the early phase of OAE 1a (corresponding to segment Ap3/C3 of the carbon-isotope curve). Cooling interludes are registered within the Selli Level, especially across segments Ap4/C4 to Ap5/C5. The interval represented by the uppermost part of the Selli Level (segment Ap6/C6), suggests that a pronounced cooling episode was followed by another cold snap after deposition of sediments just above the Selli Level. In the overlying interval (Ap7/C7), the TI shows relatively high-amplitude fluctuations. The NI indicates that the highest surface-water fertility was recorded in the lower part of the Selli Level (segments Ap3/C3 to base of Ap5/C5). The rest of the Selli Level shows low NI. Fertility started to increase in the Ap7/C7 interval.

At **Piobbico** (Fig. 4), the TI shows the warmest temperatures in the lowermost part of the recovered Selli Level corresponding to base of Ap5/C5. All samples in the Ap5/C5–Ap6/C6 interval are barren of calcareous nannofossils and therefore the TI cannot be used for relative palaeotemperature fluctuations. Corresponding to segments Ap7/C7–Ap9, a general cooling is detected (Ap8), interrupted by a brief warming. Then, from Ap9, a warming continued through most of Ap11. The rest of the late Aptian was characterized by a prolonged cooling episode (from top of Ap11 to top of Ap15) followed, at the end of the Aptian, by a warming trend showing two temperature peaks coinciding with the 113 Level and the Kilian Level at the Aptian/Albian boundary. The earliest Albian (Al1–Al3) shows a brief relative cooling immediately after the Kilian temperature spike, followed by a general warming.

The NI exhibits relatively high values in the interval immediately preceding the Selli Level and in its lowermost portions, corresponding to the base of Ap5/C5. All samples in the Ap5/C5–Ap6/C6 interval are barren of calcareous nannofossils and therefore the NI cannot be used for illustrating palaeofertility fluctuations. Above the Selli Level, a long interval of increased fertility (Ap7–Ap11) shows maximum values in the Ap9–Ap10 interval. The *Nannoconus truittii* acme is characterized by low surface-water fertility, followed by a relative increase of the NI up to Ap15. The Aptian/Albian boundary interval is marked by a decrease of the NI interrupted by a relative increase through the Kilian Level. The lowermost Albian (Al2–Al3) exhibits a trend to increased fertility extending through the Albian (Tiraboschi et al., 2009).

At **DSDP Site 463** (Fig. 5), the TI indicates warm temperatures just before and at the onset of OAE 1a. The warmest temperatures are reached at the level of segment Ap3/C3. Relative cooling interludes are registered within the Selli Level Equivalent, in segments Ap4/C4 and Ap5/C5. During the late Aptian, a long cooling (Ap7–Ap14) is registered with the coolest temperatures recorded from the top of Ap12 to the base of Ap13. The NI indicates relatively high values in the interval preceding the Selli Level Equivalent. Two maxima are recorded in the Ap3/C3 and at the base of Ap5/C5, respectively. Low NI is detected in the rest of the Selli Level Equivalent. An increase of the NI starts in Ap7 and continues up to the base of Ap12, with a maximum corresponding to Ap8. A decrease is then recorded during the *Nannoconus truittii* acme interval, followed by a relative increase.

4.3 Oxygen isotope fluctuations

The three oxygen-isotope records are somewhat scattered, and probably reflect a contribution from diagenetic cement. However, $\delta^{18}\text{O}$ trends are reproduced at the three studied sites independently of lithology, and nannofossil preservation is persistently moderate; we conclude, therefore, that the oxygen-isotope records contain a primary palaeotemperature signal only marginally modified by lithification. The main trends (Figs. 3-5) are summarized as follows:

Along segments Ap1/C1 and Ap2/C2 the isotopic ratios are relatively stable, being $\sim -2\text{‰}$ at DSDP Site 463, -1.5‰ at Piobbico and -1‰ at Cismon. At the end of segment Ap2/C2 values start to decrease, reaching -4‰ in correspondence with the negative carbon-isotope excursion (segment Ap3/C3). At Cismon, the decreasing trend is interrupted by a short-lived (~ 35 ky) interval of higher values (-1.5‰). At segment Ap4/C4, the $\delta^{18}\text{O}$ values start increasing and in the middle part of the Selli Level (segment Ap5/C5) they fluctuate: between -1 and -2‰ at Cismon, between -1 and -3‰ at Piobbico, and between -1 and -4‰ at DSDP Site 463. Corresponding with segment Ap6/C6, $\delta^{18}\text{O}$ values are relatively stable between -1 and -2‰ . Starting from segment Ap7/C7, oxygen isotopes illustrate progressively increasing ratios reaching $\sim -1\text{‰}$ around the *Nannoconus truittii* acme interval and then decrease to a minimum of $\sim -3\text{‰}$ close to the Aptian/Albian boundary. With respect to coeval sediments in the Tethys and Pacific Ocean, we notice that the oxygen-isotope values of the Cismon are greater by 1‰ .

4.4 TEX₈₆

A total of 32 samples from the Cismon core have been analyzed for TEX₈₆ of which 17 contained detectable amounts of GDGTs (Tab. 7). TEX₈₆ data for a number of sediments were excluded as they contained relatively mature organic matter, i.e. the hopane 22S/(22S+22R) ratio was >0.2 (van Breugel et al., 2007) at which level TEX₈₆ values will become biased towards lower temperatures (Schouten et al., 2004). Nearly all sediments have BIT values < 0.3 , suggesting relatively low input of soil-derived GDGTs, and thus no bias of the TEX₈₆ (Weijers et al., 2006). The values obtained for the OAE 1a interval (Figs. 2, 8) comprise one sample having a TEX₈₆ value of 0.57 indicative of $\sim 22^\circ\text{C}$ sea-surface temperature (SST) and corresponding to the most negative $\delta^{13}\text{C}$ values (segment Ap3/C3). The rest of segment Ap3/C3 is characterized by values from 0.67 to 0.61 (SST = ~ 24 to 27°C). Segments Ap4/C4 and Ap5/C5 are characterized by relatively stable values lying between 0.66 and 0.64 (SST =

~25–26°C). Corresponding to segment Ap6/C6, one sample gives a TEX₈₆ value of 0.58 (SST = ~22.5°C) and the following one of 0.64 (SST = ~25.5°C).

5 Discussion

5.1 Long- and short-term temperature fluctuations during the Aptian

Long-term temperature variations are comparable with the results of previous studies based on various temperature proxies (i.e. calcareous nannofossils, palynomorph, oxygen isotopes, and TEX₈₆). The high-resolution sampling and the stratigraphic calibration of the studied sections, enabled better constraints on long-term temperature changes and detected short-term variability improving the characterization of climate changes during the Aptian.

Long-term temperature fluctuations. A warming pulse (Fig. 7), starting at the time of the “nannoconid crisis”, characterized the onset of OAE 1a. The highest temperatures are recorded in the core of the negative carbon-isotope interval (segment Ap3/C3), as also documented in other sections in the Tethys (e.g. Menegatti et al., 1998; Hochuli et al., 1999; Luciani et al., 2001; Bellanca et al., 2002; Jenkyns, 2003; Millán et al., 2009; Erba et al., 2010; Jenkyns, 2010; Keller et al., 2011; Stein et al., 2011; Bottini et al., 2012; Hu et al., 2012; Husinec et al., 2012), Vocontian Basin (e.g. Moullade et al., 1998; Kuhnt et al., 2011), Boreal Realm (Mutterlose et al., 2010; Bottini and Mutterlose, 2012; Pauly et al., 2013; Mutterlose and Bottini, 2013), eastern European Russian Platform (Zakharov et al., 2013), and Pacific Ocean (e.g. Jenkyns, 1995; Price, 2003; Schouten et al., 2003; Ando et al., 2008; Bottini et al., 2012). Warm conditions persisted through OAE 1a, although fluctuations are detected, as discussed below. A major cooling, coeval with segment Ap7/C7, marks the end of global anoxia; it is followed by a warm phase preceding a major long-lasting cooling episode starting during segment Ap8 and extending through most of the late Aptian. Minimum temperatures were reached soon after the *N. truittii* acme, confirming the cooling (of ~4°C down to ~28°C) indicated by TEX₈₆ reconstructed from the Proto-North Atlantic (McAnena et al., 2013). Further evidence of significant cooling during the late Aptian derives from the occurrence of the Boreal (cold water) species *R. parvidentatum* at low latitudes as documented here for the Piobbico core and DSDP Site 463 (Figs. 4, 5, 7), and in the Vocontian Basin, North Sea and Proto-North Atlantic Ocean (Herrle and Mutterlose 2003, Rückheim et al., 2006; Herrle et al., 2010; McAnena et al., 2013). Close to the Aptian/Albian

boundary, temperatures show a relative increase, with warm peaks at the 113 level and Kilian equivalent.

Climate variability during OAE 1a The integration of nannofossil TI and oxygen-isotope data allows the identification of a sequence of synchronous temperature variations labelled A to M (Fig. 8) at the three studied sites. After a warming pulse at the onset of OAE 1a (Interval A), a brief (~35 ky) cooling interlude interrupted warm conditions corresponding to the interval of minimum $\delta^{13}\text{C}$ values (Interval B). It was followed by a maximum warming in the core of segment Ap3/C3 (Interval C). A cooling episode (Interval D) coincides with segment Ap4/C4 and base Ap5/C5. Intermediate climatic conditions, including one minor cooling episode (Interval E), a warm interlude (Interval F) and another minor cooling (Interval G), characterize segment Ap5/C5. Warmer temperatures (Interval H) preceded a more prominent cooling (Interval I) correlating with the latest part of OAE 1a and corresponding with segment Ap6/C6. The end of anoxia was marked by a short-lived warming (Interval L) and a further major cooling (Interval M) coinciding with the onset of segment Ap7/C7. A cool snap across segment Ap4/C4 interrupting the main warming has also been detected in the Vocontian Basin (Kuhnt et al., 2011; Lorenzen et al., 2013), Tethys (Menegatti et al., 1998; Luciani et al., 2001; Stein et al., 2011), and Turkey (Hu et al., 2012).

The correlation of oxygen-isotope and calcareous nannofossil datasets with SST estimates from TEX_{86} is difficult since the TEX_{86} data available for OAE 1a have a much lower resolution and provide relatively scattered records. The new TEX_{86} data for the Cismon core are suggestive of SSTs ranging between 22°C and 27°C. The lowermost data point, which corresponds to Interval B, indicates an SST of ~22°C which is the coolest value for the studied interval and well matches with cooler conditions reconstructed from other data. The SST values for the following three data points are rather puzzling: two indicate temperatures of ~23–25 °C and fall in Interval C - the warmest of OAE 1a - while the third data point shows almost 27°C although it falls in Interval D, interpreted to correspond to a time of relative cooling. The rest of the samples, encompassing Intervals E to H, and representing minor temperature fluctuations, fall between 25°C and 27°C. We identify one more discrepancy in the relatively low estimated SST (22.5 °C) for one sample falling in Interval H, suggested by TI and oxygen isotopes to be a relatively warm interlude.

Another problem of the TEX_{86} data of the Cismon core is related to the SSTs, which are ~5°C to 8°C lower compared with the TEX_{86} records from other sites. TEX_{86} data from DSDP Site

463 cover the Ap4/C4 to Ap6/C6 interval and range between 31°C and 34°C (recalibrated from Schouten et al., 2003 using Eq. 2). At Shatsky Rise, temperatures fall between 30°C and 35°C (recalibrated values from Dumitrescu et al., 2006 using Eq. 2). Here, two cooling interludes are detected: the first cooling of 4°C down to 30°C was during segment Ap4/C4 and corresponds to the cooling of our Interval D. The second cooling of 5°C down to 30°C seems to corresponds to segment Ap6/C6 and possibly reflects the cooling of Interval I. In the Lower Saxony Basin, SSTs indicate a distinctive warming during OAE 1a (segment C3-C6), with TEX₈₆ temperature estimates of 31–34°C. The TEX₈₆ data for the interval following OAE 1a (the C7 segment) reveal stable SSTs around 30°C (Mutterlose et al., 2010).

We notice that although the temperature variability ($\Delta = \sim 4\text{--}5^\circ\text{C}$) is similar in all sites, at Cismon the absolute temperatures are generally 5°C to 8 °C lower than at DSDP Site 463, Shatsky Rise and Lower Saxony Basin. For Cismon, also the highest (coolest temperature) $\delta^{18}\text{O}$ values are $\sim 1\text{‰}$ greater than those registered at DSDP Site 463 and $\sim 0.5\text{‰}$ greater than those at Piobbico. Generally cooler temperatures for Cismon could be explained by different latitudinal settings, the Cismon site being at $\sim 30^\circ\text{N}$, the Shatsky Rise at an almost equatorial position and the DSDP Site 463 at $\sim 20^\circ\text{S}$. However, this seems not to apply to the Boreal section (39°N) characterized by the highest ($\sim 35^\circ\text{C}$) SST. Another possible explanation for this discrepancy may be that the TEX₈₆ values from the Cismon core are already affected by the higher level of thermal maturity (i.e. hopane 22S/(22S+22R) ratios of 0.1–0.2). It has been documented that destruction of GDGTs during thermal maturation processes results in lower TEX₈₆ values due to the fact that GDGTs with cyclopentane moieties are thermally less stable (Schouten et al., 2004). Finally, it has been shown in several modern settings that TEX₈₆, although calibrated against sea-surface temperature, may sometimes reflect changes in subsurface water temperatures as well (e.g. Huguet et al., 2007; Lopes dos Santos et al., 2010), possibly because the source organisms, Thaumarchaeota, also reside in the deeper thermocline where nutrients such as ammonia might be available.

5.2 Long- and short term changes in surface water fertility

The nannofossil NI exhibits similarities between the three studied sites (simplified in Fig. 7, where nannofossil data are calibrated against the $\delta^{13}\text{C}$ curve, adopting the timescale of Malinverno et al., 2012). The earliest Aptian (segments Ap1/C1 and Ap2/C2) is characterized by low to intermediate NI values suggestive of oligotrophic conditions. The onset of OAE 1a

was marked by increasing fertility, which reached a maximum in the core interval of the negative carbon-isotope excursion (segment Ap3/C3). A decrease in surface-water fertility characterized the rest of the Selli Level (segments Ap4/C4–Ap6/C6). A shift to meso- to eutrophic conditions is detected from segment Ap8 to the beginning of the *N. truittii* acme interval, corresponding to minimal fertility conditions. The latest Aptian is then characterized by intermediate NI values, continuing into the earliest Albian.

The early Aptian has been generally seen as a time of warm and humid climate, mainly responsible for accelerated continental weathering, and consequent important nutrient fluxes to the ocean sustaining high productivity (e.g. Leckie et al., 2002; Erba, 2004; Föllmi 2012). It has also been proposed that higher fertility in the global ocean was triggered directly by submarine igneous events that introduced enormous quantities of biolimiting metals within hydrothermal plumes (e.g. Larson and Erba, 1999; Leckie et al., 2002; Erba, 2004).

Peaks in the NI are detected at the levels of the “nannoconid decline” (~1 Ma before OAE 1a) and the “nannoconid crisis”. This relationship is in agreement with the interpretation of nannoconids as oligotrophic taxa, which suffered during episodes of increased surface-water fertility. The results of the FA and PCCA analysis also support this affinity for nannoconids. Their virtual absence during the early phase of OAE 1a has been interpreted as the result of widespread meso- to eutrophic conditions (e.g. Coccioni et al., 1992; Bralower et al., 1994; Erba, 1994, 2004; Premoli Silva et al., 1999) combined with excess CO₂ in the ocean–atmosphere system (Erba and Tremolada, 2004; Erba et al., 2010).

As far as the OAE 1a interval is concerned, the fluctuations in surface-water fertility reconstructed in our work are in agreement with other studies on calcareous nanofossils from the Tethys, Boreal Realm and Atlantic Ocean. Furthermore, other proxies, for example palynomorphs (Hochuli et al., 1999) and phosphorus (e.g. Föllmi et al., 2006; Föllmi and Gainon, 2008; Stein et al., 2012), support this interpretation.

5.3 Climate and environmental changes and their relation to igneous–tectonic events during the Aptian

Our data confirm a relationship between major volcanic episodes and climate change, with associated (or subsequent) perturbations in ocean chemistry, structure and fertility. Specifically, the construction of the OJP LIP, documented in the Os-isotopic record (Tejada et

al., 2009; Bottini et al., 2012), Pb isotopes (Kuroda et al., 2011), and biomarkers (Méhay et al. 2009), suggestive of a stepwise accumulation of volcanogenic CO₂ in the atmosphere (Fig. 6). correlates in time with OAE 1a and was marked by global warming at the onset of the mid-Cretaceous greenhouse (e.g. Larson and Erba, 1999; Jenkyns, 2003). A short-lived event of possible methane hydrate dissociation probably promoted a ~100 kyr-long interval of accelerated continental weathering, temporarily reducing the CO₂ concentrations and inducing a subsequent cooling interlude (~35 ky). The next interval, marked by a maximum warming, coincided with the beginning of the most intense volcanic phase of OJP (Bottini et al., 2012). This correspondence is suggestive for a (super)greenhouse climate triggered by excess volcanogenic CO₂. The rest of OAE 1a was accompanied by climate variability including cooling interludes. Termination of widespread anoxia–dysoxia coincided with the end of the main emplacement of the OJP (Bottini et al., 2012) and a major cooling.

Large-scale igneous–tectonic events took place also during the late Aptian, but their causal impact on climate changes are less obvious, since palaeotemperatures were generally cooler. We notice that submarine volcanism (construction of OJP, Manihiki Plateau, Hikurangi Plateau, the early phase of Kerguelen Plateau) correlates with global warming, but subaerial volcanism (Kerguelen Plateau LIP) was associated with relatively cool conditions (Fig. 7). In addition to magmatic fluxes of different orders of magnitude (lower for Kerguelen, see Eldholm and Coffin, 2000), subaerial volcanism probably injected ashes and gases into the atmosphere inducing short-term cooling associated with individual degassing phases. Feedbacks related to atmospheric CO₂ drawdown via accelerated weathering were probably most significant, as also suggested by Ca isotopes (Blättler et al., 2012). On the basis of pedogenic calcretes from South Korea, Hong and Lee (2012) documented a decrease in CO₂ concentrations from ~1000 to ~500 ppmV for an interval in the late Aptian corresponding, as discussed above, to relatively cooler temperatures. However, these data present a large uncertainty in the age assignment. Recently published data by Li et al. (2014) from similar continental facies in south-east China spanning the same age, are suggestive of higher values. Specifically, here we present (Fig. 7) a revised plot of Li et al. (2014) data based on the Malinverno et al. (2012) time scale, which indicate progressively increasing CO₂ concentrations from ~1000 up to ~2000 ppmV across the *N. truittii* acme interval despite a general cooling trend. In correspondence of the lowest temperatures reached in the latest Aptian, CO₂ estimates decrease to ~1600 ppmV. The following early Albian warming trend was instead paralleled by increasing CO₂ concentrations up to 2600 ppm.

The long-lasting cool conditions of the late Aptian have been recently quantified using TEX₈₆ data (McAnena et al., 2013), which indicate a total decrease of palaeotemperatures of ~ 4°C (from 32°C to 28°C) in the equatorial Proto-Atlantic Ocean followed by a warming (~4°C) linked to the earliest Albian OAE 1b. The trends of our nannofossil TI curve are similar to these TEX₈₆-reconstructed SST changes (Fig. 7), so we adopt the values of McAnena et al. (2013) to estimate climate variations through the Aptian using the nannofossil TI fluctuations. The warming at the onset of OAE 1a corresponds to an increase of 2–3°C and climate variability during OAE 1a is marked by a cooling of ~2°C. The prominent cooling at the end of global anoxia corresponds to a decrease of ~3°C, followed by a warming of ~3°C and the coolest interval in the late Aptian is marked by a further decrease of ~4°C. As far as OAE 1a is concerned, the SST variability estimated from the TI (2–3 °C) differs little from the direct TEX₈₆ estimates of 4–5 °C.

Volcanically linked climate change seems closely connected to nutrient recycling and ocean fertilization. Different eruption styles and duration, as well as magma composition and quantity, presumably produced diverse weathering rates and introduction of biolimiting metals. Although calcareous nannoplankton are but one group of primary producers and they thrive under oligotrophic–mesotrophic conditions, the nannofossil NI can be used to trace the trophic levels of surface waters in the past. Figure 7 suggests that nutrient availability was strongly coupled with climate change in the early Aptian, but less so in the late Aptian. Fertility fluctuations could be due to differential weathering rates. During OAE 1a, greenhouse conditions generated by repetitive volcanogenic CO₂ emissions (e.g. Méhay et al., 2009; Erba et al., 2010) might have increased weathering rates, and thereby the supply of nutrients. We see a correspondence between maximum warming and high surface-water fertility. In addition, the largest submarine volcanic pulses at the beginning of OAE 1a and in the mid–late Aptian seem to have introduced biolimiting metals during submarine plateau construction. The nutrients presumably stimulated primary productivity with consequent consumption of oxygen through organic matter and metal oxidation, hence promoting anoxic conditions. The upper part of the Selli Level has high TOC content, indicating that productivity and/or preservation of organic matter was relatively high. The apparent oligotrophic conditions suggested by the NI are explained by biomarker data and nitrogen stable isotopes, indicating N-fixing cyanobacteria as the likely main primary producers during

OAE 1a (Kuypers et al., 2004; Dumitrescu and Brassell, 2006). Their N-fixation potentially provided N nutrients for the rest of the oceanic biota and presumably was the key-process in the production of organic matter, maintaining higher productivity through OAE 1a. The accumulation and burial of organic matter would have progressively acted as storage for excess CO₂, leading to lower temperatures and, possibly, to the termination of OAE 1a under less active (or ceased) OJP volcanism. We notice that the two more intense cooling interludes across OAE 1a correspond to levels with relatively high TOC content (>4%), suggesting that the burial of organic matter may have acted as a reservoir for excess CO₂, thus temporarily mitigating greenhouse conditions.

Among Cretaceous calcareous nannofloras, nannoconids are interpreted as specific to the lower photic zone, associated with a deep nutricline, so that they thrived when surface waters were characterized by oligotrophic conditions (Erba, 1994, 2004). The record of nannoconid distribution compared with the nannofossil NI confirms this hypothesis for the entire Aptian interval: the “nannoconid crisis” correlates with an increase of the NI, while the return of nannoconids following deposition of the Selli Level and the *N. truittii* acme corresponds to minima in the NI curve. We stress the fact that nannoconid abundance does not unequivocally correlate with climate change, at least in the Aptian, because the “nannoconid crisis” coincides with major warming while the final nannoconid disruption (the end of the *N. truittii* acme) corresponds to the most severe cooling.

These data contradict the interpretation of McAnena et al. (2013) for the nannoconid failure due to cold conditions in the late Aptian and imply a different explanation for abundance changes of these rock-forming nannofossils. We believe that volcanically induced CO₂ concentrations played a key role for nannoconid calcification, regardless of climatic conditions (Erba, 2006). Both the OJP and Kerguelen LIPs emitted huge quantities of CO₂ that arguably provoked ocean acidification. We emphasize that the prolonged cooling in the late Aptian promoted CO₂ absorption in the ocean and acidification. The nannoconid crises, including their final collapse in the latest Aptian, could thus be viewed as failures in biocalcification. Similarly, the major reduction in size, decrease in abundance, and species turnover documented for planktonic foraminifers (Huber and Leckie, 2011), which is coeval with the final nannoconid decline and a nannofossil turnover, might be the response of calcareous zooplankton to volcanically triggered ocean acidification.

6 Conclusions

- Quantitative study of calcareous nannofossils integrated with oxygen-isotope and TEX₈₆ records from the Tethys and Pacific Oceans has provided a reconstruction of the climatic evolution through the entire Aptian. The excellent stratigraphic time control on the studied sections coupled with high sampling density, allows confirmation of some of the climatic variations detected in previous work and highlights, during OAE 1a, temperature fluctuations not previously detected

The results from the Tethys and Pacific Oceans confirm climatic variability through the Aptian, characterized by a warming trend that began prior to and reached a maximum during OAE 1a, coincident in time with the negative carbon-isotope excursion. The rest of OAE 1a was marked by subsequent cold snaps and a further cooling took place when the uppermost part of the Selli Level was being deposited. A cooling marked the end of global anoxia and another long-lasting cooling characterized the middle late Aptian, culminating soon after the *N. truittii* acme. The latest Aptian was, instead, characterized by a gradual warming accorded by nannofossil assemblages and TEX₈₆ data. SSTs from TEX₈₆ are suggestive of 24–27 °C in the Tethys during OAE 1a, which are nevertheless 5°C to 8 °C lower than estimates from the Pacific Ocean and Boreal Realm, being probably affected by maturity levels or other factors. Although the earliest Aptian was characterized by oligotrophic conditions, the onset of OAE 1a was marked by increasing fertility, which reached a maximum at a time corresponding to the core of the negative carbon-isotope excursion. A decrease in surface-water fertility is recorded from the younger part of the Selli Level. A shift to warm and meso- to eutrophic conditions is detected after OAE 1a up to the beginning of the *N. truittii* acme interval, corresponding to minimal fertility conditions. The latest Aptian was then characterized by intermediate fertility, continuing into the earliest Albian.

- Our data indicate that the beginning of the prolonged volcanic phase during OAE 1a coincided with the warmest temperatures and the highest surface-water fertility. Weathering and hydrothermal activity were the main drivers of nutrient input, positively affecting meso- to eutrophic taxa but having a negative impact on oligotrophic species such as nannoconids, which were not greatly affected by climatic changes. Rapid ‘cold snaps’ are detected when OJP volcanism apparently continued, suggestive of feedback mechanisms, drawing down CO₂ and affecting the climate. The end of anoxia was in phase with diminished OJP activity and global cooling. We hence see a direct

relationship between OJP volcanism and climatic changes in the interval encompassing OAE 1a.

We suggest that OJP volcanism directly caused general global warming, while the excess burial of organic matter acted as an additional and/or alternative process to weathering, causing CO₂ drawdown and consequent climate change during OAE 1a. Massive subaerial volcanism (Kerguelen Plateau LIP) which took place during the late Aptian, was associated with relatively cool conditions, implying the dominant effect of atmospheric CO₂ drawdown via accelerated weathering.

Appendix A: Taxonomy

Calcareous nannofossils cited in this work:

Biscutum Black in Black and Barnes, 1959

Biscutum constans (Górka 1957) Black in Black and Barnes, 1959

Cretarhabdus Bramlette and Martini, 1964

Cretarhabdus surirellus (Deflandre, 1954) Reinhardt, 1970

Discorhabdus Noël, 1965

Discorhabdus rotatorius (Bukry 1969) Thierstein 1973

Eprolithus Stover, 1966

Eprolithus floralis (Stradner, 1962) Stover, 1966

Nannoconus Kamptner, 1931

Repagulum Forchheimer, 1972

Repagulum parvidentatum (Deflandre and Fert, 1954) Forchheimer, 1972

Rhagodiscus Reinhardt, 1967

Rhagodiscus asper (Stradner, 1963) Reinhardt, 1967

Stauroolithites Caratini, 1963

Stauroolithites stradneri (Rood et al., 1971) Bown, 1998

801 *Watznaueria* Reinhardt, 1964

802 *Watznaueria barnesiae* (Black, 1959) Perch-Nielsen, 1968

803 *Zeugrhabdotus* Reinhardt, 1965

804 *Zeugrhabdotus diplogrammus* (Deflandre in Deflandre and Fert, 1954) Burnett in Gale et
805 al., 1996

806 *Zeugrhabdotus erectus* (Deflandre in Deflandre and Fert, 1954) Reinhardt, 1965

807

808

809 **References**

810 Ando, A., Kaiho, K., Kawahata, H., and Kakegawa, T.: Timing and magnitude of early
811 Aptian extreme warming: Unraveling primary $\delta^{18}\text{O}$ variation in indurated pelagic
812 carbonates at Deep Sea Drilling Project Site 463, central Pacific Ocean. *Palaeogeogr.*
813 *Palaeocl.*, 260, 463–476, 2008.

814 Bellanca, A., Claps, M., Erba, E., Masetti, D., Neri, R., Premoli Silva, I., Venezia, F.:
815 Orbitally induced limestone/marlstone rhythms in the Albian-Cenomanian Cismon section
816 (Venetian region, northern Italy): sedimentology, calcareous and siliceous plankton
817 distribution, elemental and isotope geochemistry. *Palaeogeogr. Palaeocl.*, 126, 227–260,
818 1996.

819 Bellanca, A., Erba, E., Neri, R., Premoli Silva, I., Sprovieri, M., Tremolada, F., and Verga,
820 D.: Paleoceanographic significance of the Tethyan Livello Selli (Early Aptian) from the
821 Hyblan Formation, northwestern Sicily: biostratigraphy and high-resolution
822 chemostratigraphic records. *Palaeogeogr. Palaeocl.*, 185, 175–196, 2002.

823 Bernoulli, D. and Jenkyns, H.C.: Ancient oceans and continental margins of the Alpine-
824 Mediterranean Tethys: deciphering clues from Mesozoic pelagic sediments and ophiolites.
825 *Sedimentology*, 56, 149–190, 2009.

826 Blättler, C.L., Jenkyns, H.C., Reynard, L.M., Handerson, G.M., Significant increases in
827 global weathering during Oceanic Anoxic Events 1a and 2 indicated by calcium isotopes.
828 *Earth Planet. Sc. Lett.*, 309, 77–88, 2011.

- 829 Bottini, C. and Mutterlose, J.: Integrated stratigraphy of Early Aptian black shales in the
830 Boreal Realm: calcareous nannofossil and stable isotope evidence for global and regional
831 processes. *Newsl. Stratigr.*, 45, 115–137, 2012.
- 832 Bottini C., Cohen A.S., Erba E., Jenkyns H.C., and Coe A.L.: Osmium-isotope evidence for
833 volcanism, weathering and ocean mixing during the early Aptian OAE 1a. *Geology*, 40,
834 583–586, 2012.
- 835 Bornemann, A., Pross, J., Reichelt, K., Herrle, J. O., Hemleben, C., and Mutterlose, J.:
836 Reconstruction of short term palaeoceanographic changes during the formation of the Late
837 Albian-Niveau Breistroffer- black shales (Oceanic Anoxic Event 1d, SE France). *J. Geol.*
838 *Soc.* 162, 623–639, 2005.
- 839 Bralower, T.J., Sliter, W.V., Arthur, M.A., Leckie, R.M., Allard, D.J., Schlanger, S.O.:
840 Dysoxic/anoxic episodes in the Aptian-Albian (Early Cretaceous), in: *The Mesozoic*
841 *Pacific: Geology, Tectonics and Volcanism*, edited by: Pringle, M., Sager, W.W., Sliter,
842 W.V., Stein, S., *Am. Geophys. Union Geophys. Mon.* 77, 5–37, 1993.
- 843 Bralower, T.J., Arthur, M.A., Leckie, R.M., Sliter, W.V., Allard, D.J., and Schlanger, S.O.:
844 Timing and paleoceanography of oceanic dysoxia/anoxia in the late Barremian to early
845 Aptian. *Palaios*, 9, 335–369, 1994.
- 846 Bralower, T.J., Leckie, R.M., Sliter, W.V., Thierstein, H.R.: An integrated Cretaceous
847 microfossil biostratigraphy, in: *Geochronology Time Scales and Global Stratigraphic*
848 *Correlation*, edited by: Berggren, W.A., Kent, D.V., Aubry, M.P., Hardenbol, J., *Soc. Econ.*
849 *Paleontol. Mineral. Spec. Publ.*, 54, 65–79, 1995.
- 850 Bralower, T.J., Cobabe, E., Clement, B., Sliter, W.V., Osburne, C., and Longoria, J.: The
851 record of global change in mid-Cretaceous, Barremian-Albian sections from the Sierra
852 Madre, northeastern Mexico. *J. Foraminiferal Res.*, 29, 418–437, 1999.
- 853 Channell, J.E.T., Erba, E., Muttoni, G., and Tremolada, F.: Early Cretaceous magnetic
854 stratigraphy in the APTICORE drill core and adjacent outcrop at Cismon (Southern Alps,
855 Italy), and the correlation to the proposed Barremian/Aptian boundary stratotype. *Bull.*
856 *Geol. Soc. Am.*, 112, 1430–1443, 2000.
- 857 Coccioni, R., Nesci, O., Tramontana, M., Wezel, C.F., and Moretti, E.: Descrizione di un
858 livello-guida “Radiolaritico-Bituminoso-Ittiolitico” alla base delle Marne a Fucoidi
859 nell’Appennino Umbro-Marchigiano. *Boll. Soc. Geol. Ital.*, 106, 183–192, 1987.

- 860 Coccioni, R., Erba, E., and Premoli Silva, I.: Barremian-Aptian calcareous plankton
861 biostratigraphy from the Gorgo a Cerbara section (Marche, Central Italy) and implication
862 for planktonic evolution. *Cret. Res.*, 13, 517–537, 1992.
- 863 De Lurio, J.L. and Frakes, L.A.: Glendonites as a paleoenvironmental tool: implications for
864 early Cretaceous high latitude climates in Australia. *Geochim. Cosmochim. Ac.* 63,
865 1039–1048, 1999.
- 866 Dumitrescu, M. and Brassell, S.C.: Compositional and isotopic characteristics of organic
867 matter for the early Aptian oceanic anoxic event at Shatsky Rise, ODP leg 198.
868 *Palaeogeogr. Palaeoclimatol.*, 235, 168–191, 2006.
- 869 Dumitrescu, M., Brassell, S.C., Schouten, S., Hopmans, E.C. and Sinninghe Damsté, J.S.:
870 Instability in tropical Pacific sea-surface temperatures during the early Aptian. *Geology*,
871 34, 833–866, 2006.
- 872 Eldholm, O. and Coffin, M.F.: Large Igneous Provinces and plate tectonics, in: *The History*
873 *and Dynamics of Global Plate Motion*, edited by: Richards, M., Gordon, R., and van der
874 Hilst, R. *Geophysical Monograph*, 121, Washington, DC (American Geophysical Union),
875 309–326, 2000.
- 876 Erba, E.: Aptian-Albian calcareous nannofossil biostratigraphy of the Scisti a Fucoidi cored at
877 Piobbico (central Italy). *Riv. Ital. Paleontol. Stratigr.*, 94, 249–284, 1988.
- 878 Erba, E.: Calcareous nannofossil distribution in pelagic rhythmic sediments (Aptian-Albian
879 Piobbico core, central Italy). *Riv. Ital. Paleontol. Stratigr.*, 97, 455–484, 1992a.
- 880 Erba, E.: Middle Cretaceous calcareous nannofossils from the Western Pacific (ODP Leg
881 129). Evidence for paleoequatorial crossing: *Proc. ODP Sci. Res.*, 129, 189–201, 1992b.
- 882 Erba, E.: Nannofossils and superplumes: the early Aptian nannoconid crisis.
883 *Paleoceanography*, 9, 483–501, 1994.
- 884 Erba, E.: Calcareous nannofossils and Mesozoic oceanic anoxic events. *Mar. Mic.*, 52, 85–
885 106, 2004.
- 886 Erba, E.: The first 150 million years history of calcareous nannoplankton: Biosphere–
887 geosphere interactions. *Palaeogeogr. Palaeoclimatol.*, 232, 237–250, 2006.
- 888 Erba, E. and Larson, R.: The Cismon Apticore (Southern Alps, Italy): Reference section for
889 the Lower Cretaceous at low latitudes. *Riv. Ital. Paleontol. Stratigr.*, 104, 181–192, 1998.

890 Erba, E. and Tremolada, F.: Nannofossil carbonate fluxes during the Early Cretaceous:
 891 phytoplankton response to nutrification episodes, atmospheric CO₂ and anoxia:
 892 *Paleoceanography*, 19, 1–18, 2004.

893 Erba, E., Channell, J.E.T., Claps, M., Jones, C., Larson, R.L., Opdyke, B., Premoli Silva, I.,
 894 Riva, A., Salvini, G., and Torricelli, S.: Integrated stratigraphy of the Cismon Apticore
 895 (Southern Alps, Italy): a reference section for the Barremian-Aptian interval at low
 896 latitudes. *J. Foraminiferal Res.*, 29, 371–391, 1999.

897 Erba, E., Bottini, C., Weissert, J.H., and Keller, C.E.: Calcareous Nannoplankton Response to
 898 Surface-Water Acidification Around Oceanic Anoxic Event 1a. *Science*, 329, 428–432,
 899 2010.

900 Erba E., Duncan R.A., Bottini C., Tiraboschi D., Weissert H., Jenkyns H.C., Malinverno, A.:
 901 Environmental Consequences of Ontong Java Plateau and Kerguelen Plateau Volcanism.
 902 GSA Special Paper, under final review by the editor.

903 Föllmi, K.B.: Early Cretaceous life, climate and anoxia. *Cret. Res.*, 35, 230–257, 2012.

904 Föllmi, K.B. and Gainon, F.: Demise of the northern Tethyan Urgonian carbonate platform
 905 and subsequent transition towards pelagic conditions. The sedimentary record of the Col de
 906 la Plaine Morte area, central Switzerland. *Sedimentary Geology*, 205, 142–159, 2008.

907 Föllmi, K.B., Godet, A., Bodin, S., and Linderl, P.: Interactions between environmental
 908 change and shallow water carbonate buildup along the northern Tethyan margin and their
 909 impact on the Early Cretaceous carbon isotope record. *Paleoceanography*, 21, PA4211,
 910 doi: 10.1029/2006PA001313, 2006.

911 Frakes, L. A. and Francis, J. E.: A guide to Phanerozoic cold polar climates from high-latitude
 912 ice-rafting in the Cretaceous. *Nature*, 333, 547–549, 1988.

913 Habermann, A. and Mutterlose, J.: Early Aptian black shales from NW Germany: calcareous
 914 nannofossil and their paleoceanographic implications: *Geol. Jahrbuch A*, 212, 379–400,
 915 1999.

916 Herrle, J.O.: Paleoceanographic and paleoclimatic implications on mid-Cretaceous black
 917 shale formation in the Vocontian Basin and the Atlantic. Evidence from calcareous
 918 nannofossils and stable isotopes. *Tubingen Mikropalaontologische Mitteilungen*, 27, 1–
 919 114, 2002.

920 Herrle, J.O.: Reconstructing nutricline dynamics of Mid-Cretaceous oceans: Evidence from
 921 calcareous nannofossils from the Niveau Paquier black shale (SE France). *Mar.*
 922 *Micropaleontol.*, 47, 307–321, 2003.

923 Herrle, J.O. and Mutterlose, J.: Calcareous nannofossils from the Aptian–Lower Albian
 924 southeast France: paleoecological and biostratigraphic implication. *Cret. Res.*, 24, 1–22,
 925 2003.

926 Herrle, J.O., Pross, J., Friedrich, O., Kössler, P., and Hemleben, C.: Forcing mechanisms for
 927 Mid-Cretaceous black shale formation: Evidence from the upper Aptian and lower Albian
 928 of the Vocontian Basin (SE France). *Palaeogeogr. Palaeoclimatol.*, 190, 399–426, 2003.

929 Herrle, J.O., Köbller, P., Friedrich, O., Erlenkeuser, H., Hemleben C.: High resolution carbon
 930 isotope records of the Aptian to Lower Albian from SE France and the Mazagan Plateau
 931 (DSDP Site 545): a stratigraphic tool for paleoceanographic and paleobiologic
 932 reconstruction. *Earth Planet. Sc. Lett.*, 218, 149–161, 2004.

933 Herrle, J.O., Kosler, P., and Bollmann, J.: Palaeoceanographic differences of early Late
 934 Aptian black shale events in the Vocontian Basin (SE France). *Palaeogeogr. Palaeoclimatol.*,
 935 297, 367–376, 2010.

936 Hochuli, P.A., Menegatti, A.P., Weissert, H., Riva, A., Erba E., and Premoli Silva, I.:
 937 Episodes of high productivity and cooling in the early Aptian Alpine Tethys. *Geology*, 27
 938 (7), 657–660, 1999.

939 Hong, S.K. and Lee, Y.I.: Evaluation of atmospheric carbon dioxide concentrations during the
 940 Cretaceous. *Earth Planet. Sc. Lett.*, 23-28, 328–327, 2012.

941 Hopmans, E. C., J. W. H. Weijers, E. Schefuß, L. Herfort, J. S. Sinninghe Damsté, and S.
 942 Schouten: A novel proxy for terrestrial organic matter in sediments based on branched and
 943 isoprenoid tetraether lipids. *Earth Planet. Sci. Lett.*, 224, 107–116, 2004.

944 Hu, X., Kuidong, Z., Yilmaz, I.O., and Yongxiang, L.: Stratigraphic transition and
 945 palaeoenvironmental changes from the Aptian oceanic anoxic event 1a (OAE1a) to the
 946 oceanic red bed 1 (ORB1) in the Yenicesihlar section, central Turkey. *Cret. Res.*, 38,
 947 40–51, 2012.

948 Huber, B.T. and Leckie, R.M.: Planktic foraminiferal species turnover across deep-sea
 949 Aptian/Albian boundary sections. *J. Foraminiferal Res.*, 41, 53–95, 2011.

- 950 Huguet, C., Schimmelmann, A., Thunell, R., Lourens, L.J., Sinninghe Damsté, J.S., Schouten,
951 S.: A study of the TEX86 paleothermometer in the water column and sediments of the
952 Santa Barbara Basin, California. *Paleoceanography* 22, PA3203, doi:
953 10.1029/2006PA001310, 2007.
- 954 Husinec, A., Harman, C.A., Regan, S.P., Mosher, D.A., Sweeney, R.J., and Read, J.F.:
955 Sequence development influenced by intermittent cooling events in the Cretaceous Aptian
956 greenhouse, Adriatic platform, Croatia. *AAPG Bulletin*, 96, no. 12, 2215–2244, 2012.
- 957 Jenkyns, H.C.: Carbon-isotope stratigraphy and paleoceanographic significance of the Lower
958 Cretaceous shallow-water carbonates of resolution Guyot, Mid-Pacific Mountains, in:
959 Proceedings of the Ocean Drilling Program Scientific Results, edited by: Winterer, E.L.,
960 Sager, W.W., Firth, J.V., Sinton, J.M., College Station, Texas, 143, 99–104, 1995.
- 961 Jenkyns, H.C.: Evidence for rapid climate change in the Mesozoic–Palaeogene greenhouse
962 world. *Philos. T. Roy. Soc., Ser. A* 361, 1885–1916, 2003.
- 963 Jenkyns, H.C.: Geochemistry of oceanic anoxic events. *Geochem. Geophys. Geo*, 11, Q03004,
964 doi: 10.1029/2009GC002788, 2010.
- 965 Jenkyns, H.C. and Wilson, P.A.: Stratigraphy, paleoceanography, and evolution of Cretaceous
966 Pacific guyots: relics from a greenhouse Earth. *Am. J. Sci.* 299, 341–392, 1999.
- 967 Jenkyns, H.C., Schouten-Huibers, L., Schouten, S., and Sinninghe Damsté, J.S.: Warm
968 Middle Jurassic–Early Cretaceous high-latitude sea-surface temperatures from the
969 Southern Ocean. *Clim. Past*, 8, 215–226, 2012.
- 970 Jones, C.E. and Jenkyns, H.C.: Seawater strontium isotopes, oceanic anoxic events, and
971 seafloor hydrothermal activity in the Jurassic and Cretaceous. *American Journal of*
972 *Science*, 301, 112–149, 2001.
- 973 Keller, C.E., Hochuli, P.A., Weissert, H., Weissert, H., Bernasconi, S.M., Giorgioni, M., and
974 Garcia, T.I.: A volcanically induced climate warming and floral change preceded the onset
975 of OAE1a (Early Cretaceous). *Palaeogeogr. Palaeoclimatol.*, 305, 43–49, 2011.
- 976 Kemper, E.: Das Klima der Kreide-Zeit. *Geol. Jahrbuch A*, 96, 5–185, 1987.
- 977 Kim, J.-H., van der Meer, J., Schouten, S., Helmke, P., Willmott, V., Sangiorgi, F., Koç, N.,
978 Hopmans, E. C., and Sinninghe Damsté, J.S.: New indices and calibrations derived from

979 the distribution of crenarchaeal isoprenoid tetraether lipids: Implications for past sea
980 surface temperature reconstructions, *Geochim. Cosmochim. Ac.*, 74, 4639–4654, 2010.

981 Kuhnt, W., Holbourn, A., and Moullade, M.: Transient global cooling at the onset of early
982 Aptian oceanic anoxic event (OAE) 1a. *Geology*, 39, 323–326, 2011.

983 Kuroda, J., Tanimizu, M., Hori, R.S., Suzuki, K., Ogawa, N.O., Tejada, M.L.G., Coffin, M.F.,
984 Coccioni, R., Erba, E., Ohkouchi, N.: Lead isotopic record of Barremian-Aptian marine
985 sediments: Implications for large igneous provinces and the Aptian climatic crisis. *Earth*
986 *Planet. Sc. Lett.*, 307, 126–134, 2011.

987 Kuypers, M.M.M., van Breugel, Y., Schouten, S., Erba, E., and Sinninghe Damsté, J.S.: N₂-
988 fixing cyanobacteria supplied nutrient N for Cretaceous oceanic anoxic events. *Geology*,
989 32, 853–856, 2004.

990 Larson, R.L.: Geological consequences of superplumes. *Geology*, 19, 963–966, 1991.

991 Larson, R.L. and Erba, E.: Onset of the mid-Cretaceous greenhouse in the Barremian-Aptian:
992 Igneous events and the biological, sedimentary and geochemical responses.
993 *Paleoceanography*, 14, 663–678, 1999.

994 Leckie, R.M., Bralower, T.J., and Cashman, R.: Oceanic anoxic events and plankton
995 evolution: Biotic response to tectonic forcing during the Mid-Cretaceous.
996 *Paleoceanography*, 17, PA1041, doi: 10.1029/2001PA000623, 2002.

997 Li, X., Jenkyns, H.C., Zhang, C., Wang, Y., Liu, L., and Cao, K.: Carbon isotope signatures
998 of pedogenic carbonates from SE China: rapid atmospheric $p\text{CO}_2$ changes during middle–
999 late Early Cretaceous time. *Geological Magazine*, in press,
1000 doi:10.1017/S0016756813000897, 2014.

1001 Lopes dos Santos, R., Prange, M., Castañeda, I.S., Schefuß, E., Mulitza, S., Schulz, M.,
1002 Niedermeyer, E.M., Sinninghe Damsté, J.S., and Schouten S.: Glacial-interglacial
1003 variability in Atlantic Meridional Overturning Circulation and thermocline adjustments in
1004 the tropical North Atlantic. *Earth Plan. Sci. Lett.*, 300, 407–414, 2010.

1005 Lorenzen, J., Kuhnt, W., Holbourn, A., Flögel, S., Moullade, M., and Tronchetti, G.: A new
1006 sediment core from the Bedoulian (Lower Aptian) stratotype at Roquefort-La Bédoule, SE
1007 France. *Cret. Res.*, 39, 6–16, 2013.

1008 Luciani, V., Cobianchi, M., and Jenkyns, H.C.: Biotic and geochemical response to anoxic
1009 events: the Aptian pelagic succession of the Gargano Promontory (southern Italy).
1010 *Geological Magazine*, 138, 277–298, 2001.

1011 Mahanipour, A., Mutterlose, J., Kani, A.L., and Adabi, M.H.: Palaeoecology and
1012 biostratigraphy of early Cretaceous (Aptian) calcareous nannofossils and the delta C-
1013 ¹³(carb) isotope record from NE Iran. *Cret. Res.*, 32, 331–356, 2011.

1014 Malinverno, A., Erba, E., Herbert, T.D.: Orbital tuning as an inverse problem: Chronology of
1015 the early Aptian oceanic anoxic event 1a (Selli Level) in the Cismon APTICORE.
1016 *Paleoceanography*, 25, PA2203, doi: 10.1029/2009PA001769, 2010.

1017 Malinverno, A., Hildebrandt, J., Tominaga, M., and Channell, J.E.T.: M-sequence
1018 geomagnetic polarity time scale (MHTC12) that steadies global spreading rates and
1019 incorporates astrochronology constraints. *J. Geophys. Res.*, 117, B06104, doi:
1020 10.1029/2012JB009260, 2012.

1021 Malkoč, M., Mutterlose, J., and Pauly, S.: Timing of the Early Aptian $\delta^{13}\text{C}$ excursion in the
1022 Boreal Realm. *Newsl. Stratigr.*, 43, 251–273, 2010.

1023 Marshall, J.D.: Climatic and oceanographic isotopic signals from the carbonate rock record
1024 and their preservation. *Geol. Mag.*, 129, 143–160, 1992.

1025 Maurer, F., van Buchem, F.S.P., Eberli, G.P., Pierson, B.J., Raven, M.J., Larsen, P., Al-
1026 Hussein, M.I., and Vincent, B.: Late Aptian long-lived glacio-eustatic lowstand recorded
1027 on the Arabian Plate. *Terra Nova*, 00, 1–8, 2012.

1028 McAnena, A., Flögel, S., Hofmann, P., Herrle, J.O., Griesand, A., Pross, J., Talbot, H.M.,
1029 Rethemeyer, J., Wallmann, K., and Wagner, T.: Atlantic cooling associated with a marine
1030 biotic crisis during the mid-Cretaceous period. *Nat. Geosci.*, 6, 558–651, 2013.

1031 Méhay, S., Keller, C.E., Bernasconi, S.M., Weissert, H., Erba, E., Bottini, C., and Hochuli,
1032 P.A.: A volcanic CO₂ pulse triggered the Cretaceous Oceanic Anoxic Event 1a and a
1033 biocalcification crisis. *Geology*, 37, 819–822, 2009.

1034 Mélières, F., Deroo, G., and Herbin, J.P.: Organic-matter-rich and hypersiliceous Aptian
1035 sediments from western Mid-Pacific Mountains. *Deep Sea Drilling Project Leg 62, Initial*
1036 *Rep. Deep Sea Drill. Proj.*, 62, 903–915, 1978.

- 1037 Menegatti, A.P., Weissert, H., Brown, R.S., Tyson, R.V., Farrimond, P., Strasser, A., and
1038 Caron, M.: High-resolution $\delta^{13}\text{C}$ -stratigraphy through the early Aptian Livello Selli of the
1039 Alpine Tethys. *Paleoceanography*, 13, 530–545, 1998.
- 1040 Millán, M.I., Weissert, H.J., Fernandez-Mendiola, P.A., and Garcia-Mondejar, J.: Impact of
1041 Early Aptian carbon cycle perturbations on evolution of a marine shelf system in the
1042 Basque-Cantabrian Basin (Aralar, N Spain). *Earth Planet. Sc. Lett.*, 287, 392–401, 2009.
- 1043 Moullade, M., Kuhnt, W., Berger, J.A., Masse, J., and Tronchetti, G.: Correlation of
1044 biostratigraphic and stable isotope events in the Aptian historical stratotype of La Bedoule
1045 (southern France). *Comptes Rendus de l'Academie des Sciences, serie II*, 327, 693–698,
1046 1998.
- 1047 Mutterlose, J.: Temperature-controlled migration of calcareous nannofloras in the north-west
1048 European Aptian, in: *Nannofossils and their applications*, edited by Crux, J.A. and van
1049 Heck, S.E., Ellis Horwood, Chichester, England, 122–142, 1989.
- 1050 Mutterlose, J.: Migration and evolution patterns of floras and faunas in marine Early
1051 Cretaceous sediments of NW Europe. *Palaeogeogr. Palaeoclimatol.*, 94, 261–282, 1992.
- 1052 Mutterlose, J. and Bottini, C.: Early Cretaceous chalks from the North Sea giving evidence for
1053 global change. *Nat. Commun.*, 4, 1686, 1–6, 2013.
- 1054 Mutterlose, J., Bornemann, A., and Herrle, J.O.: Mesozoic calcareous nannofossils - state of
1055 the art. *Palaontologische Zeitschrift*, 79, 113–133, 2005.
- 1056 Mutterlose, J., Bornemann, A., and Herrle, J.: The Aptian – Albian cold snap: Evidence for
1057 “mid” Cretaceous icehouse interludes. *N. Jb. Geol. Paläont. Abh.* 252, 217–225, 2009.
- 1058 Mutterlose J., Malkoč, M., Schouten, S., Sinninghe Damsté, J. S., and Forster, A.: TEX_{86} and
1059 stable $\delta^{18}\text{O}$ paleothermometry of early Cretaceous sediments: Implications for belemnite
1060 ecology and palaeotemperature proxy application. *Earth Planet. Sc. Lett.*, 298, 286–298,
1061 2010.
- 1062 Pauly, S., Mutterlose, J. and Wray, D.S.: *Palaeoceanography of Lower Cretaceous*
1063 (Barremian–Lower Aptian) black shales from northwest Germany evidenced by calcareous
1064 nannofossils and geochemistry. *Cret. Res.*, 42, 28–43, 2013.
- 1065 Petrizzo, M.R., Huber, B.T., Gale, A.S., Barchetta, A., and Jenkyns, H.C.: Abrupt planktic
1066 foraminiferal turnover across the Niveau Kilian at Col de Pré-Guittard (Vocontian Basin,

- 1067 southeast France): new criteria for defining the Aptian/Albian boundary. *Newsl. Stratigr.*,
1068 45, 55–74, 2012.
- 1069 Premoli Silva, I., Ripepe, M., and Tornaghi, M.E.: Planktonic foraminiferal distribution
1070 record productivity cycles: evidence from the Aptian-Albian Piobbico core (central Italy).
1071 *Terra Nova*, 1, 443–448, 1989a.
- 1072 Premoli Silva, I., Erba, E., and Tornaghi, M.E.: Paleoenvironmental signals and changes in
1073 surface fertility in mid-Cretaceous Corg-rich pelagic facies of the Furoid Marls (central
1074 Italy). *Geobios, Mémoire Spécial*, 11, 225–236, 1989b.
- 1075 Premoli Silva, I., Erba, E., Salvini, G., Verga, D., and Locatelli, C.: Biotic changes in
1076 Cretaceous anoxic events. *J. Foraminiferal Res.*, 29, 352–370, 1999.
- 1077 Price, G.D.: The evidence and implications of polar ice during the Mesozoic. *Earth-Science*
1078 *Reviews*, 48, 183–210, 1999.
- 1079 Price, G.D.: New constraints upon isotope variation during the early Cretaceous (Barremian-
1080 Cenomanian) from the Pacific Ocean. *Geological Magazine*, 140, 513–522, 2003.
- 1081 Price, G.D., Williamson, T., Henderson, R.A., and Gagan, M.K.: Barremian–Cenomanian
1082 palaeotemperatures for Australian seas based on new oxygen-isotope data from belemnite
1083 rostra. *Palaeogeogr. Palaeocl.*, 358–360, 27–39, 2012.
- 1084 Pucéat, E., Lécuyer, C., Sheppard, S.M., Dromart, G., Reboulet, S., and Grandjean, P.:
1085 Thermal evolution of Cretaceous Tethyan marine waters inferred from oxygen isotope
1086 composition of fish tooth enamels. *Paleoceanography* 18, 1029, doi: 10.1029/
1087 2002PA000823, 2003.
- 1088 Roth, P. H.: Mid-Cretaceous calcareous nannoplankton from the central Pacific: implications
1089 for Paleocanography *Init. Rep. Deep Sea Drill. Proj.*, 62, 471–489, 1981.
- 1090 Roth, P.H. and Krumbach, K.R.: Middle Cretaceous calcareous Nannofossil biogeography
1091 and preservation in the Atlantic and Indian oceans: implication for paleogeography. *Mar.*
1092 *Mic.*, 10, 235–266, 1986.
- 1093 Rückheim, S., Bornemann, A., and Mutterlose, J.: Planktic foraminifera from the mid-
1094 Cretaceous (Barremian-Early Albian) of the North Sea Basin: Palaeoecological and
1095 palaeoceanographic implications. *Mar. Mic.* 58, 83–102, 2006.

- 1096 Schouten, S., Hopmans, E.C., Schefuss, E., and Sinninghe Damsté, J.S.: Distributional
1097 variations in marine crenarchaeotal membrane lipids: A new organic proxy for
1098 reconstructing ancient sea water temperatures?. *Earth Planet. Sc. Lett.*, 204, 265–274,
1099 2002.
- 1100 Schouten, S., Hopmans, S., Forster, A., Van Breugel, Y., Kuypers, M.M.M., and Sinninghe
1101 Damsté, J.S.: Extremely high sea-surface temperatures at low latitudes during the middle
1102 Cretaceous as revealed by archaeal membrane lipids. *Geology*, 31, 1069–1072, 2003.
- 1103 Schouten, S., Hopmans, E.C., and Sinninghe Damsté, J.S.: The effect of maturity and
1104 depositional redox conditions on archaeal tetraether lipid palaeothermometry, *Org.*
1105 *Geochem.*, 35, 567–571, 2004.
- 1106 Schouten, S., Huguet, C., Hopmans, E.C., Kienhuis, M.V.M. and Sinninghe Damsté, J.S.:
1107 Analytical methodology for TEX₈₆ paleothermometry by high-performance liquid
1108 chromatography/atmospheric pressure chemical ionization-mass spectrometry. *Anal.*
1109 *Chem.*, 79, 2940–2944, 2007.
- 1110 Sinninghe Damsté, J.S., Hopmans, E.C. Schouten, S. van Duin, A.C.T., and Geenevasen
1111 J.A.J.: Crenarchaeol: the characteristic core glycerol dibiphytanyl glycerol tetraether
1112 membrane lipid of cosmopolitan pelagic crenarchaeota. *J. Lipid Res.*, 43, 1641–1651,
1113 2002.
- 1114 Stein, M., Föllmi, K.B., Westermann, S., Godet, A., Adatte, T., Matera, V., Fleitmann, D.,
1115 and Berner, Z.: Progressive palaeoenvironmental change during the Late Barremian-Early
1116 Aptian as prelude to Oceanic Anoxic Event 1a: Evidence from the Gorgo a Cerbara section
1117 (Umbria-Marche basin, central Italy). *Palaeogeogr. Palaeocl.*, 302, 396–406, 2011.
- 1118 Stein, M., Westermann, S., Adatte, T., Matera, V., Fleitmann, D., Spangenberg, J.E., Föllmi,
1119 K.B.: Late Barremian–Early Aptian palaeoenvironmental change: The Cassis-La Bédoule
1120 section, southeast France. *Cret. Res.*, 37, 209–222, 2012.
- 1121 Tejada, M.L.G., Katsuhiko S., Kuroda, J., Coccioni, R., Mahoney, J.J., Ohkouchi, N.,
1122 Sakamoto, T., and Tatsumi, Y.: Ontong Java Plateau eruption as a trigger for the early
1123 Aptian oceanic anoxic event. *Geology*, 37, 855–858, 2009.
- 1124 Thiede, J., Dean, W.E., Rea, D.K., Vallier, T.L., and Adelseck, C.G.: The geologic history of
1125 the Mid-Pacific Mountains in the central North Pacific Ocean: A synthesis of Deep-Sea
1126 Drilling studies. *Init. Rep. Deep Sea Drill. Proj.* 62, 1073–1120, 1981.

1127 Tiraboschi, D., Erba, E., and Jenkyns, H.J.: Origin of rhythmic Albian black shales (Piobbico
1128 core, central Italy) Calcareous nannofossil quantitative and statistical analysis and
1129 paleoceanographic reconstructions. *Paleoceanography*, 24, PA2222, doi:
1130 10.1029/2008PA001670, 2009.

1131 Tornaghi, M.E., Premoli Silva, I. and Ripepe, M.: Lithostratigraphy and planktonic
1132 foraminiferal biostratigraphy of the Aptian-Albian “Scisti a Fucoidi” in the Piobbico core,
1133 Marche, Italy: Background for cyclostratigraphy. *Riv. Ital. Paleontol. Stratigr.*, 95, 223–
1134 264, 1989.

1135 Tremolada, F., Erba, E., and Bralower, T.J.: Late Barremian to Early Aptian calcareous
1136 nannofossil paleoceanography and paleoecology from the Ocean Drilling Program Hole
1137 641C (Galicja Margin). *Cret. Res.*, 87, 887–897, 2006.

1138 van Breugel, Y., Schouten, S., Tsikos, H., Erba, E., Price G. D., and Sinninghe Damsté, J.S.:
1139 Synchronous negative carbon isotope shifts in marine and terrestrial biomarkers at the
1140 onset of the early Aptian oceanic anoxic event 1a: Evidence for the release of ^{13}C -depleted
1141 carbon into the atmosphere. *Paleoceanography*, 22, PA1210, doi: 10.1029/2006PA001341,
1142 2007.

1143 Watkins, D.K.: Nannoplankton productivity fluctuations and rhythmically-bedded pelagic
1144 carbonates of the Greenhorn Limestone (Upper Cretaceous). *Palaeogeogr. Palaeocl.*, 74,
1145 75–86, 1989.

1146 Weijers, J.W.H., Schouten, S., Spaargaren, O.C., and Sinninghe Damsté, J.S.: Occurrence and
1147 distribution of tetraether membrane lipids in soils: Implication for the use of the TEX86
1148 proxy and the BIT index, *Org. Geochem.*, 37, 1680–1693, 2006.

1149 Weissert, H.: C-isotope stratigraphy , a monitor of palaeoenvironmental change: a case study
1150 from the Early Cretaceous. *Surveys in Geophysics*, 10, 1–61, 1989.

1151 Weissert, H., and Lini, A.: Ice Age interludes during the time of Cretaceous greenhouse
1152 climate?, in: *Controversies in Modern Geology*, edited by: D.W. Muller, J.A. McKenzie
1153 and H. Weissert, Academic, San Diego, California, USA, 173–191, 1991.

1154 Williams, J.R. and Bralower, T.J.: Nannofossil assemblage, fine fraction stable isotopes, and
1155 the paleoceanography of the Valanginian-Barremian (Early Cretaceous) North Sea Basin,
1156 *Paleoceanography*, 10, 815–839, 1995.

Wise, S.W. Jr.: Mesozoic-Cenozoic history of calcareous nannofossils in the region of the Southern Ocean. *Palaeogeogr. Palaeoclimatol.*, 67, 157–179, 1988.

Zakharov, Y.D., Baraboshkin, E.Y., Weissert, H., Michailova, I.A., Smyshlyaeva, O.P., and Safronov, P.P.: Late Barremian–early Aptian climate of the northern middle latitudes: Stable isotope evidence from bivalve and cephalopod molluscs of the Russian Platform. *Cret. Res.*, 44, 183–201, 2013.

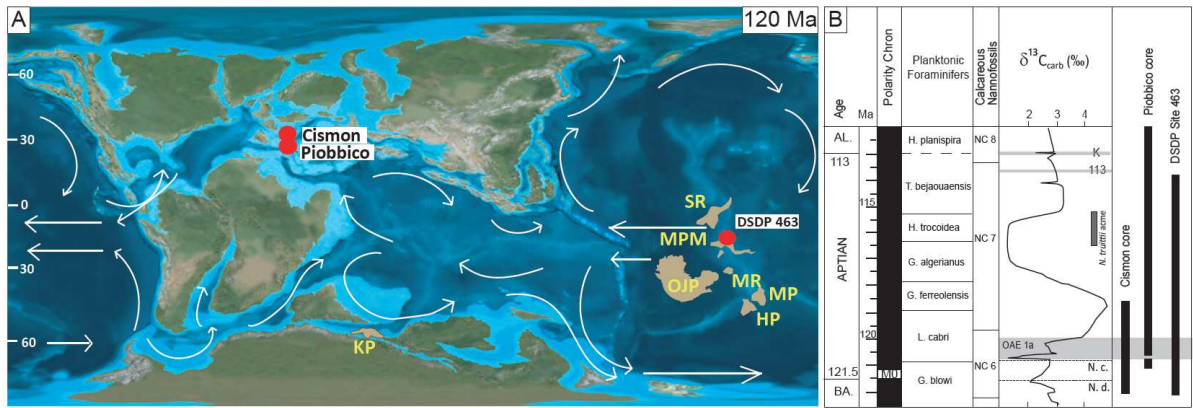


Figure 1. A) Location map of studied sites at 120 Ma (modified after Erba et al. under final review by the editor). OJP = Ontong Java Plateau; KP = Kerguelen Plateau; SR = Shatsky Rise; MPM = Mid-Pacific Mountains; MR = Magellan Rise; MP = Manihiki Plateau; HP = Hikurangi Plateau. B) Stratigraphic ranges of the studied sections. Latest Barremian to earliest Albian chronologic framework is from Erba et al. (under final review by the editor). Numerical ages are based on the timescale of Malinverno et al. (2012). K = Niveau Kilian; 113 = 113 Level; N.c. = Nannoconid crisis; N.d.= Nannoconid decline.

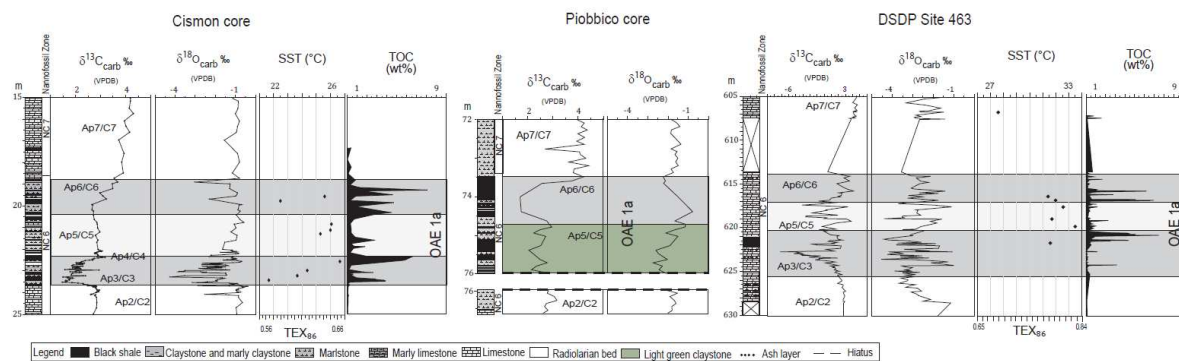


Figure 2. Correlation between the Cismon core, the Piobbico core and DSDP Site 463. $\delta^{13}\text{C}$ data after: Erba et al. (1999) and Méhay et al. (2009) for the Cismon core; Erba et al. (under final review by the editor) for the Piobbico core; Price (2003), Ando et al. (2008) and Bottini et al. (2012) for DSDP Site 463. Bulk $\delta^{18}\text{O}$ data after: Erba et al. (2010) for the Cismon core; Price (2003), Ando et al. (2008) and this work for DSDP Site 463. TOC after: Erba et al. (1999) and Bottini et al. (2012) for the Cismon core; Ando et al. (2008) for DSDP Site 463. TEX_{86} after: Schouten et al. (2003) for DSDP Site 463; this work for the Cismon core. For both cores SST was calculated using the equation of Kim et al. (2010). Grey bands indicate intervals of higher (darker) and lower (lighter) TOC values.

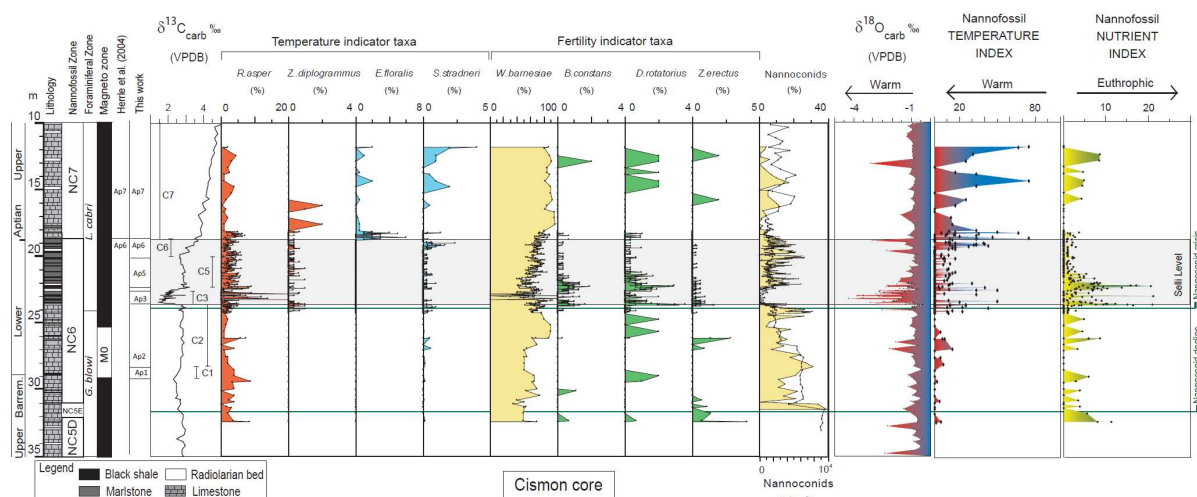


Figure 3. Cismon core: fluctuations of calcareous nannofossil temperature and fertility indicator taxa. Temperature (TI) and Nutrient (NI) indices based on calcareous nannofossils (low values of the TI indicate high temperatures and vice versa; high values of the NI indicate

high surface-water productivity and vice versa). $\delta^{13}\text{C}$ is from Erba et al. (1999) and Méhay et al. (2009). Nannofossil and foraminiferal biostratigraphy is from Erba et al. (1999). Magnetostratigraphy is from Channell et al. (2000). Bulk $\delta^{18}\text{O}$ data are from Erba et al. (2010).

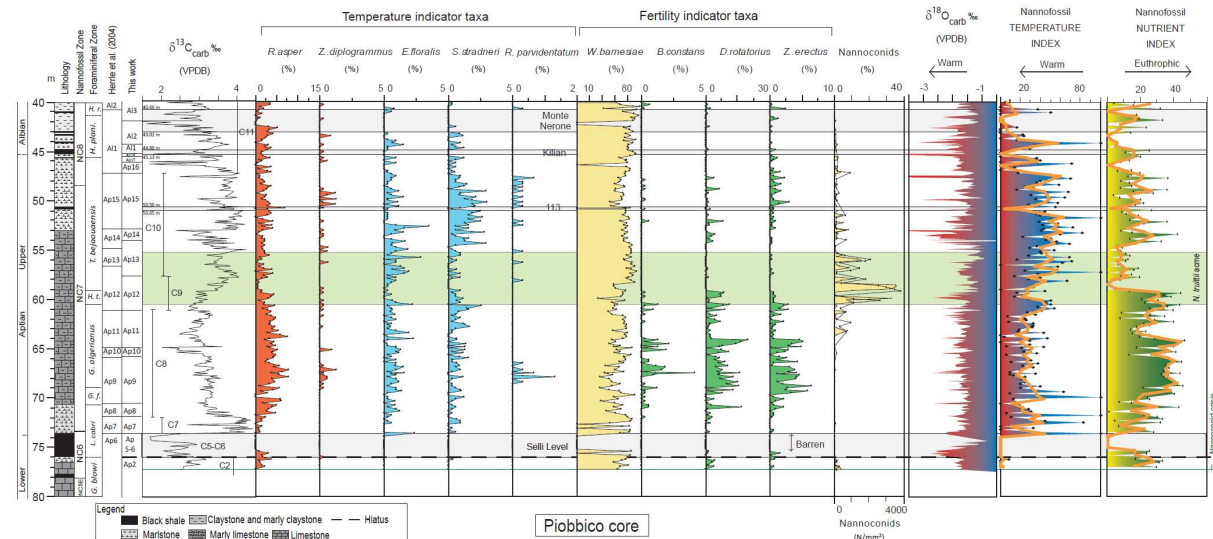


Figure 4. Piobbico core: fluctuations of calcareous nannofossil temperature and fertility indicator taxa. Temperature (TI) and Nutrient (NI) indices based on calcareous nannofossils (low values of the TI indicate high temperatures and vice versa; high values of the NI indicate high surface-water productivity and vice versa). Orange curve indicates smoothed TI and NI records based on three-point moving average. $\delta^{13}\text{C}$ is from Erba et al. (under final review by the editor). Nannofossil and foraminiferal biostratigraphy is from Erba et al. (1988) and Tornaghi et al. (1989). Bulk $\delta^{18}\text{O}$ data are from this work.

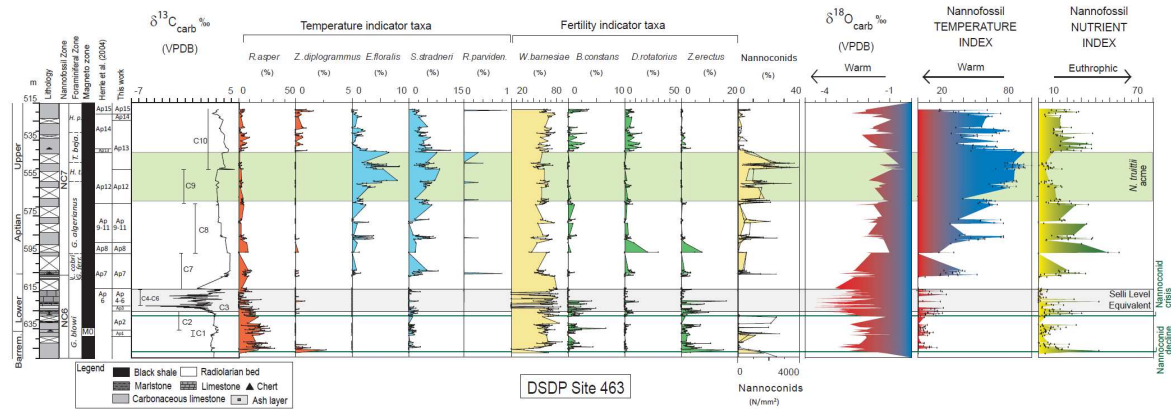


Figure 5. DSDP Site 463 Mid-Pacific Mountains: fluctuations of calcareous nannofossil temperature and fertility indicator taxa. Temperature (TI) and Nutrient (NI) indices based on calcareous nannofossils (low values of the TI indicate high temperatures and vice versa; high values of the NI indicate high surface-water productivity and vice versa). $\delta^{13}\text{C}$ is from Price (2003), Ando et al. (2008), Bottini et al. (2012). Nannofossil and foraminiferal biostratigraphy is from Erba, (1994) and Ando et al. (2008). Magnetostratigraphy is from Tarduno et al. (1989). Bulk $\delta^{18}\text{O}$ data are from Price (2003), Ando et al. (2008), and this work.

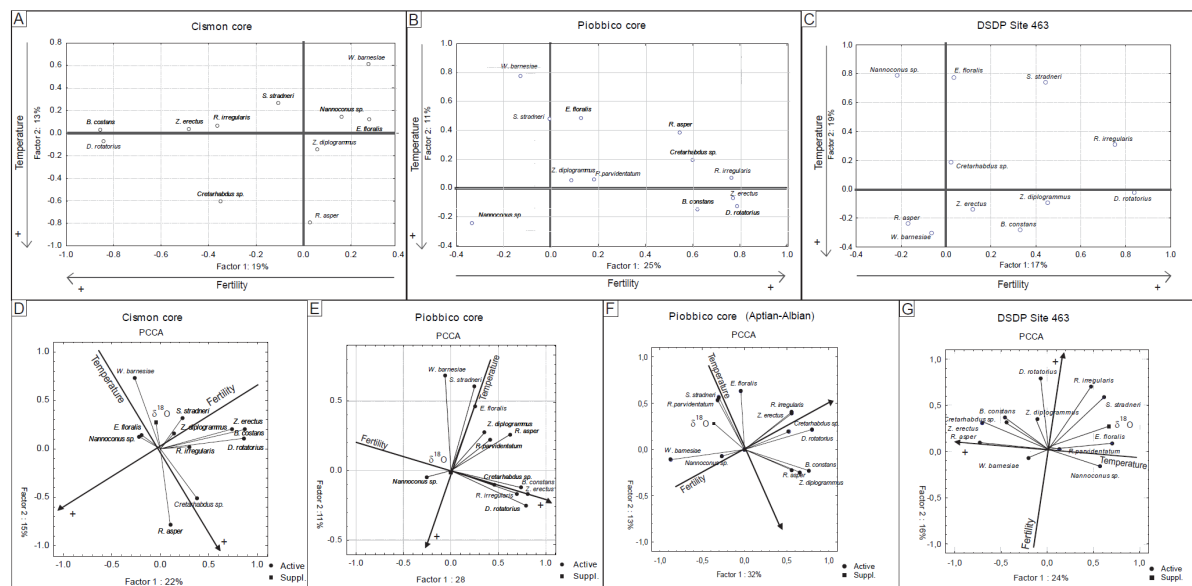


Figure 6. On the top row, the results of Factor Analysis (R-mode) varimax normalized rotation with principal component extraction are presented for (A) Cismone core, (B) Piobbico core and (C) DSDP Site 463. On the bottom row, the results of the principal component and classification analysis (PCCA) are presented for (D) Cismone core, (E) Piobbico core, (F)

Piobbico core, including the Albian dataset from Tiraboschi et al. (2009), (G) DSDP Site 463.
The associated variable is the $\delta^{18}\text{O}$.

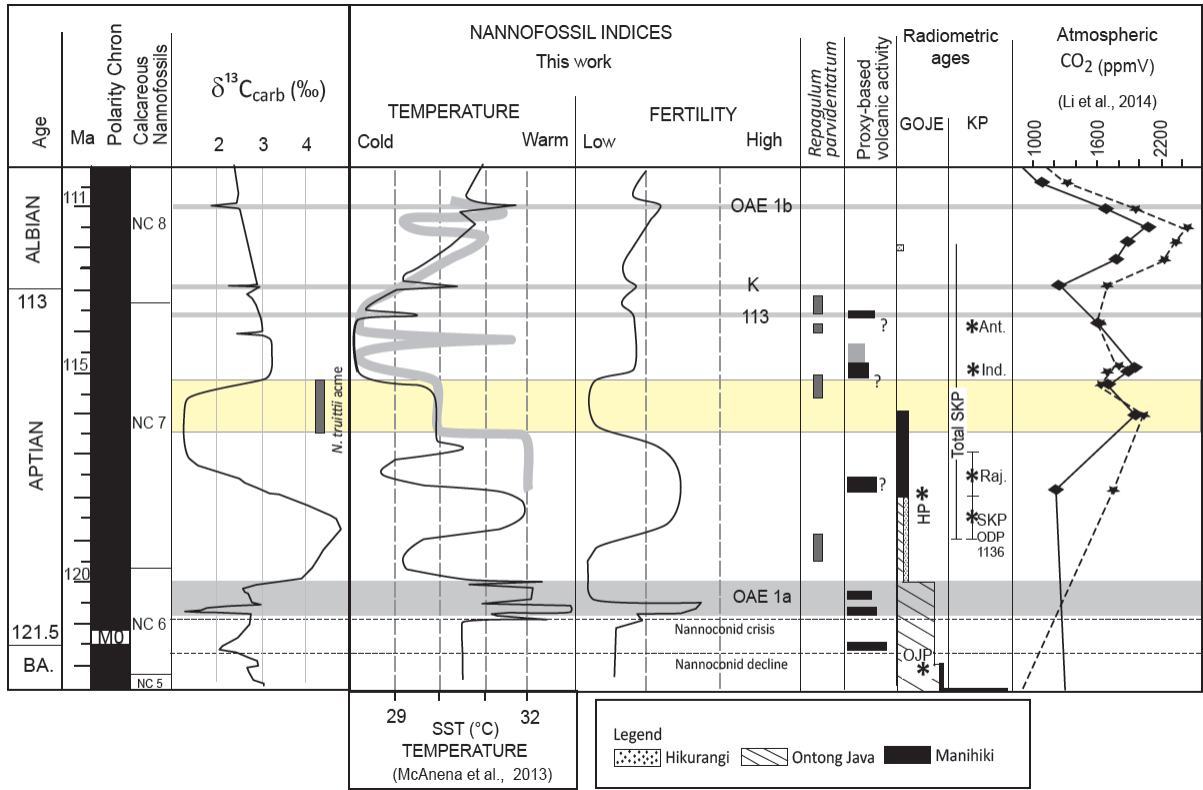


Figure 7. Nannofossil-based temperature and nutrient variations across the Aptian reconstructed in this work and across the Albian (from Tiraboschi et al., 2009). The thick-grey curve represents SST from McAnena et al. (2013). Bio-chemo-magneto stratigraphy after Erba et al. (under final review by the editor). Numerical ages are based on the timescale of Malinverno et al. (2012). Multiproxy-based volcanic phases and radiometric ages of the Greater Ontong Java Event (GOJE) and Kerguelen LIPs are from Erba et al. (under final review by the editor). Atmospheric CO₂: Li et al. (2014). Nannofossil data and isotopic data are integrated with nannofossil data from the Albian (Tiraboschi et al., 2009).

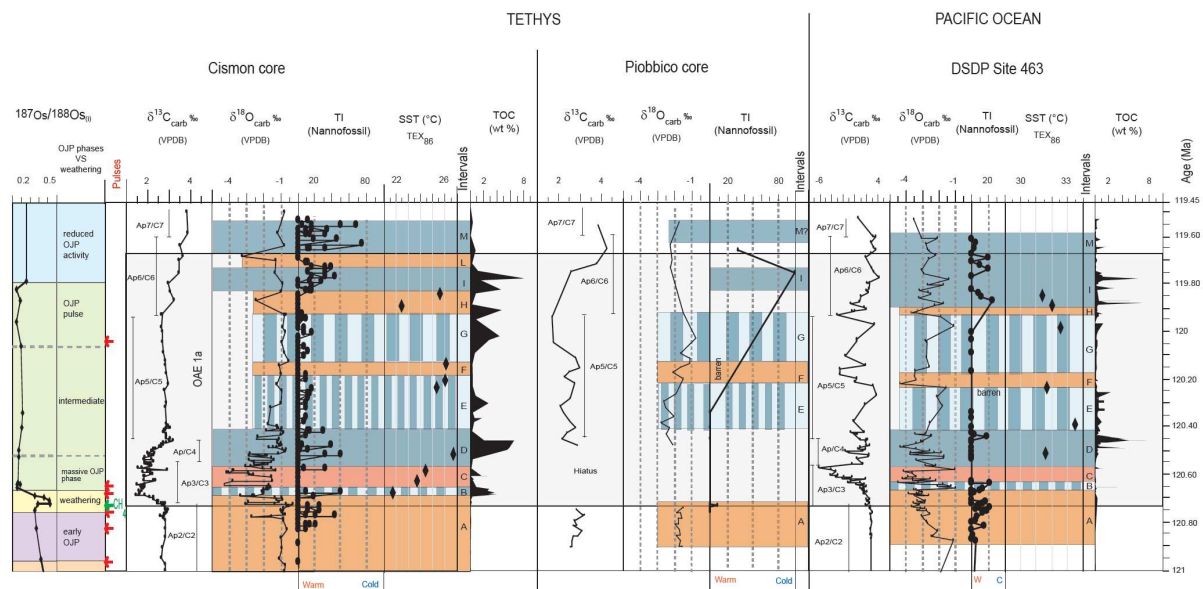


Figure 8. Nannofossil temperature index (TI), TEX_{86} , and oxygen-isotope values for the Cismon core, Piobbico core and DSDP Site 463 plotted against chemostratigraphy. The age determination is based on the cyclocronology available for the Cismon core (Malinverno et al., 2010). $\delta^{13}C$ data after: Erba et al. (1999) and Méhay et al. (2009) for the Cismon core; Erba et al. (under final review by the editor) for the Piobbico core; Price (2003), Ando et al. (2008) and Bottini et al. (2012) for DSDP Site 463. Bulk $\delta^{18}O$ data after: Erba et al. (2010) for the Cismon core; Price (2003), Ando et al. (2008) and this work for DSDP Site 463. TOC after: Erba et al. (1999) and Bottini et al. (2012) for the Cismon core; Ando et al. (2008) for DSDP Site 463. TEX_{86} after: Schouten et al. (2003) for DSDP Site 463; this work for the Cismon core (SST calculated using the equation of Kim et al., 2010). On the left is reported the Os-isotope curve (Bottini et al., 2012) and the volcanogenic CO_2 pulses (red arrows) reconstructed by Erba et al. (2010). The intervals A to M represent the climatic interludes (warming and cooling) reconstructed in this work.